

Low energy and dynamical properties of a single hole in the $t - J_z$ model

Q.F. Zhong and S. Sorella

International School for Advanced Study, Via Beirut 4, 34013 Trieste, Italy

(April 21, 2022)

Abstract

We review in details a recently proposed technique to extract information about dynamical correlation functions of many-body hamiltonians with a few Lanczos iterations and without the limitation of finite size. We apply this technique to understand the low energy properties and the dynamical spectral weight of a simple model describing the motion of a single hole in a quantum antiferromagnet: the $t - J_z$ model in two spatial dimension and for a double chain lattice. The simplicity of the model allows us a well controlled numerical solution, especially for the two chain case. Contrary to previous approximations we have found that the single hole ground state in the infinite system is continuously connected with the Nagaoka fully polarized state for $J_z \rightarrow 0$. Analogously we have obtained an accurate determination of the dynamical spectral weight relevant for photoemission experiments. For $J_z = 0$ an argument is given that the spectral weight vanishes at the Nagaoka energy faster than any power law, as supported also by a clear numerical evidence. It is also shown that spin charge decoupling is an exact property for a single hole in the Bethe lattice but does not apply to the more realistic lattices where the hole can describe closed loop paths.

75.10.Jm,75.40.Mg,71.10.+x

Typeset using REVTeX

I. INTRODUCTION

After the discovery of the high- T_c materials [1], there have been an increasing attention to the study of strongly correlated fermion systems. In his pioneer work [2] Anderson first pointed out that a doped Mott insulator, described by the one band Hubbard model, should contain the basic physics of the high- T_c superconductors. The Hubbard model was proposed independently in 1963 by Gutzwiller, Hubbard and Kanamori [3–5]. Despite of its simple-looking hamiltonian and a lot of efforts, the physics of the model is still a subject of debate.

In the large U limit, it is more convenient to use a canonical transformation to project out the doubly occupied sites, costing energy U . This leads to the so-called t - J model:

$$H = -t \sum_{\langle i,j \rangle, \sigma} (c_{i\sigma}^\dagger c_{j\sigma} + h.c.) + J \sum_{\langle i,j \rangle} (\mathbf{S}_i \cdot \mathbf{S}_j - \frac{1}{4} n_i n_j). \quad (1)$$

where the constraint of no double occupancy is understood. Here $c_i^\dagger(c_i)$ creates (annihilates) an electron at site i , $n_i = \sum_{\sigma} n_{i\sigma}$ is the corresponding density operator with $n_{i\sigma} = c_{i\sigma}^\dagger c_{i\sigma}$, the symbol $\langle i, j \rangle$ means summation over nearest neighbors, $J = \frac{4t^2}{U}$ is the superexchange coupling and finally the spin density operator \mathbf{S}_i is defined by the Pauli matrices $\vec{\sigma}$: $\mathbf{S}_i = \sum_{\sigma, \sigma'} c_{i,\sigma}^\dagger \frac{\vec{\sigma}_{\sigma, \sigma'}}{2} c_{i,\sigma'}$.

Starting from a more realistic three band Hubbard hamiltonian describing the Copper-Oxygen layer, Zhang and Rice showed that the low-energy physics of cuprate superconductors is determined by the singlet state formed by the additional hole on oxygen with the existing hole copper. [6] They also showed that the hopping of this singlet is described by an effective one-band t - J model, with J and U essentially unrelated. This makes the $t - J$ model even more appropriate to describe the Copper-Oxide planes at low energies rather than the original one-band Hubbard model.

During the last few years, a huge amount of analytical and numerical work has been devoted to the study of the $t - J$ model. [7] However the physics contained in the t - J model is far from clear because of the interplay between antiferromagnetic long range order and charge degrees of freedom. Exact numerical methods are usually limited to a very small

linear size in more than 1D and practically nothing about the low energy physics has been understood numerically.

In this paper we will make a detailed numerical study of a simplified version of the t - J model, *i.e.* neglecting the spin fluctuations in the exchange term ($\mathbf{S}_i \cdot \mathbf{S}_j \rightarrow S_i^z S_j^z$ in Eq. (1)) and considering only the properties of a single hole. Due to the simplification of the model, we are able to work directly in the infinite size system and have a satisfactory description for the low energy dynamics of a single hole in such a simple model of an antiferromagnet:

$$H = -t \sum_{\langle i,j \rangle, \sigma} (c_{i\sigma}^\dagger c_{j\sigma} + h.c.) + J_z \sum_{\langle i,j \rangle} S_i^z S_j^z. \quad (2)$$

A basic motivation of this work is to obtain reliable numerical results on this simple $t - J_z$ model since it may be useful for further investigation of the more interesting $t - J$ model. For instance, the $t - J_z$ model was often used in the past [8,9] to test several approximations on the $t - J$ model. In fact most of the physical properties of the t - J model probably remain valid even for the t - J_z model. From this point of view it is worth mentioning that the $t - J$ model and the $t - J_z$ model have the same limit for J or $J_z \rightarrow 0$ and for infinite spatial dimensions the two model coincide, since the spin fluctuations are irrelevant in this limit. [10]

The single hole problem represents certainly a further simplification but is still physically relevant, since the single particle excitations in magnetic insulators can actually be studied by the photoemission and the inverse photoemission spectroscopy.

For a single hole a rigorous theorem proven by Nagaoka is known for $J_z = 0$. The so called Nagaoka theorem states that for a bipartite finite lattice in more than one dimension ($d > 1$) the ferromagnetic state with maximum spin is the unique ground state with energy $e_N = -zt$, in any subspace with given total spin projection.

A complete description of the one hole spectrum in the $J_z = 0$ limit, not limited to the ground state, was first given in [11], where the so-called “retraceable path approximation” (RPA) was introduced. In the Ising limit as a hole hops in a Néel state, it scrambles the spins along its path. In order to return the spin configuration to its original state, it was argued

that, to a good approximation, one can consider only paths in which the hole retraces its path back to the origin, thereby returning all of the spins to their original position. In this approximation one can write down an explicit analytic solution for the Green's function:

$$G_k(\omega) = \frac{z\sqrt{\omega^2 - 4(z-1)} - (z-2)\omega}{2(\omega^2 - z^2)} \quad (3)$$

and the spectral weight $A(k, \omega) = -\frac{\text{sgn } \omega}{\pi} \text{Im} G_k(\omega)$ reads

$$A(\omega) = \frac{z\sqrt{4(z-1)t^2 - \omega^2}}{4\pi(z^2t^2 - \omega^2)} \quad (4)$$

where $z = 2d$ is the number of nearest neighbors. The spectral weight is completely incoherent and dispersionless with a one particle band, which is 75% narrower (in 3D) than the noninteracting band. The RPA is exact in 1D and for the Bethe lattice (where Nagaoka theorem does not apply), and recently it has been shown to be exact in the limit of infinite spatial dimensionality. [10]

For finite J_z/t , the competition between the kinetic energy t favoring the ferromagnetic configuration and the exchange energy J_z favoring the antiferromagnetic alignment of the neighboring spins makes the problem of particular interest. By neglecting closed loops, e.g. in the Bethe lattice case, it is possible to derive a closed solution [12,13], which we will refer in the following as the “string picture”. In the string picture, the hole moves in an antiferromagnetic spin background, leaving behind a string of overturned spins, which costs an energy proportional to the length of the path. The overturned spins behave like an effective linear potential for the hole. In the continuum limit, valid for $J_z \rightarrow 0$, the problem is reduced to a one dimensional Schrödinger equation with a linear potential $V \sim xJ_z$ where x is the length of the string.

$$H = -\sqrt{z-1}t \frac{\partial^2}{\partial x^2} + \frac{J_z(z-2)}{2}x - 2\sqrt{z-1}t. \quad (5)$$

The solution of this hamiltonian leads to a series of bound states. The hole is essentially localized with a discrete energy spectrum:

$$E_n = a_n\sqrt{z-1}t \left(\frac{J_z(z-2)}{2\sqrt{z-1}t} \right)^{2/3} - 2\sqrt{z-1}t \quad (6)$$

where a_n are the zeros of the Airy function $Ai(z)$. Recently, it has been shown that the string picture is exact up to order $\frac{1}{d^2}$, where d is the spatial dimensionality. [10]

Contrary to the $J_z = 0$ case, at finite J_z the spectral weight has δ -function peaks at energies E_n . The weight of the δ -function at the lowest energy is called the quasiparticle weight Z and is found to vanish linearly in J_z , using the continuous limit (5). [9]

Later Kane, Lee and Read [9] introduced a self-consistent Born approximation that can be considered an extension of the RPA to the more physical $t - J$ model. Their approach is widely accepted since they were able to reproduce the asymptotic behavior of the $t - J_z$ model in the string picture and a large amount of numerical work on small lattices seems to be in qualitative agreement with the predictions of this theory. [14–16]

In the retraceable path approximation or in the string picture and similarly within the self-consistent Born approximation, closed loop paths are neglected in order to simplify the analytic structure of the one hole Green's function. However, this certainly introduces an approximation even in the simple $t - J_z$ model. In fact the most important effect due to the inclusion of closed loop paths in this model was first noted by Trugman. [8] In 2D a hole can hop around a square plaquette one and half times without disturbing the spin background with a net translation to the next-nearest-neighbor along the diagonal. This means that the hole can “unwind” the string and self-generate a next-nearest-neighbor hopping. The full localization of charge carriers found within the retraceable path approximation and the string picture is an artifact of the approximation.

Another interesting issue is whether the spin and charge degrees of freedom are decoupled or not. [17,18] Spin charge decoupling is a well known phenomenon in one dimension, where a one electron excitation can be decomposed into a spinon excitation which carries spin but no charge and a holon excitation which carries charge but no spin. We will show in the present paper that spin charge decoupling is an *exact* property of the $t - J_z$ model in the Bethe lattice with arbitrary coordination number z at single hole doping and present some numerical work, ruling out the possibility of spin charge decoupling in physically relevant lattices where closed loops are allowed.

In this paper, we make use of the Lanczos method to calculate the single hole spectral function in the infinite system. We will first introduce a transformation to eliminate the charge degree of freedom to get an effective spin Hamiltonian in a given momentum subspace (Section 2). Then we will use the Lanczos method in order to diagonalize the effective spin Hamiltonian in the infinite lattice (Section 3). We will concentrate on two chains (2C) and two-dimensional (2D) square lattices. The 2C case is much easier for numerical study compared to the 2D lattice. The 2C lattice is not a trivial lattice for the t - J_z model, because it has the basic properties of an higher dimensional lattice, such as the existence of closed loop paths and the validity of the Nagaoka theorem.

Most of the above results were obtained by use of the Lanczos Spectra Decoding method. This method allows us to analyze the Lanczos data in the infinite system, where only a small number of Lanczos iterations is possible (Section 3). The validity of the Lanczos Spectra Decoding is proved analytically and numerically on the Bethe lattice (Section 4). In section 5, we will show our numerical results both for the $J_z = 0$ and finite J_z case. Finally we will discuss about the formation of a ferromagnetic polaron around the hole for small J_z , and about the analytic form of the spectral weight close to the Nagaoka energy.

II. FORMALISM

A. Effective Spin Hamiltonian

The $t - J_z$ Hamiltonian (2) is translational invariant, so the most general one-hole state with total spin $S_z^T = M_z + \frac{1}{2}$ and total momentum $-p$ (hole momentum p) can be written:

$$|\psi_p\rangle = \frac{1}{\sqrt{N}} \sum_{R,\sigma} e^{ipR} c_{R,\sigma} T_R |S_O\rangle \quad (7)$$

where $|S_O\rangle$ is a pure spin state that satisfies: i) $n_R |S_O\rangle = |S_O\rangle$ for all sites R , ii) $n_{\downarrow O} |S_O\rangle = |S_O\rangle$ *i.e.* the spin at the origin is fixed to $\sigma_0 = -\frac{1}{2}$, iii) the total spin along the z -axis is a well defined quantum number in the state $|S_O\rangle$, *i.e.* $S_z^T |S_O\rangle = M_z |S_O\rangle$.

The operator T_R in (7) is the translation operator that brings the origin O to the lattice point R . It is formally defined by:

$$T_R c_{R',\sigma} T_{-R} = c_{R+R',\sigma} \quad (8)$$

States with definite momentum $|\psi_p\rangle$ are eigenstates of T_R such that $T_R|\psi_p\rangle = e^{-ipR}|\psi_p\rangle$. Note also that the sum over σ in the definition of $|\psi_p\rangle$ in (7) is used only for later convenience.

A pure spin Hamiltonian can be derived as following. We evaluate the expectation value of the t - J_z Hamiltonian on the one-hole state $|\psi_p\rangle$, $E_p = \langle \psi_p | H | \psi_p \rangle$, and consider first the case $J_z = 0$:

$$E_p = \frac{t}{N} \sum_{R_1, R_2, R, \tau_\mu, \sigma, \sigma_1, \sigma_2} e^{-ip(R_1 - R_2)} \langle S_O | T_{-R_1} c_{R_1, \sigma_1}^\dagger \hat{P} c_{R+\tau_\mu, \sigma} c_{R, \sigma}^\dagger c_{R_2, \sigma_2} T_{R_2} | S_O \rangle \quad (9)$$

Now i) $\sigma_1 = \sigma_2$ since the total S_z^T has to be conserved in order to give a non-vanishing contribution in E_p . ii) $R = R_2$ and $R + \tau_\mu = R_1$, otherwise we create a doubly occupied site which is projected out either by \hat{P} or by overlapping with $\langle S_O |$. Finally we obtain that $E_p = \langle S_O | H_p^{eff} | S_O \rangle$ with:

$$H_p^{eff} = t \sum_{\sigma, \sigma', \tau_\mu} e^{-ip\tau_\mu} T_{-\tau_\mu} (c_{\tau_\mu, \sigma'}^\dagger c_{\tau_\mu, \sigma} c_{O, \sigma}^\dagger c_{O, \sigma'}). \quad (10)$$

H_p^{eff} acts only on spin states. In fact for $S = \frac{1}{2}$ it is possible to express the term between parenthesis in terms of spin operators only:

$$\chi_{R_i, R_j} = \sum_{\sigma, \sigma'} c_{R_i, \sigma'}^\dagger c_{R_i, \sigma} c_{R_j, \sigma}^\dagger c_{R_j, \sigma'} = \frac{1}{2} n_{R_i} n_{R_j} + 2 \mathbf{S}_{R_i} \cdot \mathbf{S}_{R_j} \quad (11)$$

Finally H_p^{eff} reads:

$$H_p^{eff} = t \sum_{\tau_\mu} e^{-ip\tau_\mu} T_{-\tau_\mu} \chi_{O, \tau_\mu} = t \sum_{\tau_\mu} e^{ip\tau_\mu} \chi_{O, \tau_\mu} T_{\tau_\mu}. \quad (12)$$

Note that the product of the operators $T_{-\tau_\mu}$ and χ_{O, τ_μ} appearing in H_p^{eff} permutes spins and leaves the origin O unchanged. Moreover, since the operator χ interchanges the spins at sites R_i and R_j , we have that $\chi_{R_i, R_j} = \chi_{R_j, R_i}$ and that $\chi_{R_i, R_j}^2 = 1$.

Analogously we can extend to $J_z \neq 0$ the derivation of a pure spin Hamiltonian and obtain:

$$H_p^{eff} = t \sum_{\tau_\mu} e^{ip\tau_\mu} \chi_{O,\tau_\mu} T_{\tau_\mu} + J_z \sum_{(i,j) \neq O} S_{R_i}^z S_{R_j}^z \quad (13)$$

The full Hamiltonian commutes with \mathbf{S}_O (since it actually does not depend on the spin at the origin) and thus it can be defined on $N - 1$ sites.

In conclusion for any eigenstate $|S_O\rangle$ of H_p^{eff} with definite $S_O^z |S_O\rangle = -\frac{1}{2} |S_O\rangle$ we have an eigenstate of the $t - J_z$ Hamiltonian written in the form (7). In fact, by use of the variational principle any eigenstate of (2) or (13) is obtained by $\frac{\delta}{\delta \psi_p} \langle \psi_p | H | \psi_p \rangle = 0$, $\frac{\delta}{\delta S_O} \langle S_O | H | S_O \rangle = 0$ with the condition $\langle \psi_p | \psi_p \rangle = 1$, $\langle S_O | S_O \rangle = 1$ respectively. Since $E_p = \langle \psi_p | H | \psi_p \rangle = \langle S_O | H_p^{eff} | S_O \rangle$ and $\langle \psi_p | \psi_p \rangle = \langle S_O | S_O \rangle$, it clearly follows that all the eigenstates of H_p^{eff} with definite spin at the origin define a true eigenstate of H by use of (7). In conclusion the one hole problem is mapped onto a diagonalization of a pure spin Hamiltonian H_p^{eff} for the given momentum p . [19] A similar effective Hamiltonian can be obtained for the t - J model, by substituting S^z with \mathbf{S} in (13).

It is interesting to note that H_p^{eff} is not translational invariant and that the momentum of the hole appears as a simple parameter. It is just this property that allow us to diagonalize the t - J_z model in certain momentum subspace in the infinite lattice.

As it is shown in the Appendix many useful dynamical quantities such as the Green's function and current operators can be easily translated in terms of spin operators acting on this spin space in which the hole is fixed at the origin.

B. Green's Function for $J_z = 0$

Following Brinkman and Rice [11], we can expand the Green's function G in terms of the momenta $\langle H | (H_p^{eff})^k | H \rangle$ of the Hamiltonian on the translation invariant ground state of the undoped system $|H\rangle$. For $J_z = 0$, at vanishing doping, the hamiltonian is classical and $|H\rangle$ is given by:

$$|H\rangle = \frac{1}{\sqrt{2}}(|N\rangle + |N'\rangle) \quad (14)$$

where $|N\rangle$ and $|N'\rangle$ are the two possible determination of the Néel state.

The one hole Green's function can be generally written as a summation of all possible paths traced by the hole during its motion on the lattice. A path is then defined by a set of coordinates $\{R_l\}^n$ with $l = 0, \dots, n$, which are connected by nearest neighbor vectors τ_μ

$$R_l - R_{l-1} = \tau_{\mu_l}. \quad (15)$$

Among all the possible paths it is useful to identify the skeleton ones. [20] A path $\{R_l\}^n$ of length n is a skeleton path if $R_{l+1} \neq R_{l-1}$ for any $l = 1, \dots, n-1$. By definition, for any skeleton path, the hole never retraces its path immediately. It is clear that all the remaining paths can be obtained by dressing each site R_l of the skeleton path by all possible retraceable paths. The retraceable paths can be then summed exactly.

Instead of giving the detailed derivation, we will present the final result and discuss some of the special cases. The most general Green's function can be written in a formal expansion of skeleton paths of length $2n$:

$$G(R, \omega) = G_{BR}(\omega) \sum_n K(\omega)^{2n} C_n(R) \quad (16)$$

where G_{BR} is the Brinkman Rice result (3), which includes only retraceable path contribution starting from the origin $R = O$ and coming back to the same site:

$$G_{BR}(\omega) = \frac{1}{\omega \left(1 - \frac{z}{z-1} \Sigma^A(\omega)\right)} = t^{-1} \frac{K(\omega)}{1 - K(\omega)^2}, \quad (17)$$

while the function $K(\omega)$ is the exact contribution of all possible retraceable paths on each site of the skeleton path different from the origin:

$$K(\omega) = \frac{t}{\omega} \frac{1}{1 - \Sigma^A(\omega)} = \frac{1}{2(z-1)t} \left[\omega - \text{sgn}(\omega) \sqrt{\omega^2 - 4(z-1)t^2} \right] \quad (18)$$

Finally in (16) the coefficients $C_n(R)$ are determined by: $C_n(R) = \sum_{\text{all skeleton } \{R_l\}^{2n}} \Omega(\{R_l\}^{2n})$, where $\Omega(\{R_l\}^n)$ are spin correlation functions, which, generally speaking, depend on the path,

$$\Omega(\{R_l\}^n) = \langle H | \chi_{R_n, R_{n-1}} \chi_{R_{n-1}, R_{n-2}} \cdots \chi_{R_1, R_0} | H \rangle \quad (19)$$

In the Ising case $\Omega(\{R_l\}^n)$ vanish for odd n and are simply equal to either zero or one for even n depending on whether the skeleton path change the Néel order or not. Instead they are complicated correlation functions in the $t - J$ model for $J \rightarrow 0$. In this case the expression (16) is still valid provided we include the odd n contributions.

Two possible limits can be exactly solved using the previous expression (16) for the Green's function.

1. Bethe Lattice Case

The Bethe lattice is defined on a Cailey-tree with coordination z and for $z = 2$ it coincides with the one dimensional chain. In the Bethe lattice there is only one path that connects two arbitrary sites of the lattice because there are no closed loops in this lattice (see e.g. [16] for a more detailed definition of the Bethe lattice). As in one dimension there is only one skeleton path connecting the origin to a given point R and $\Omega(\{R_l\}^n) = \Omega(R_n)$, which is only a function of the final position R_n . We can immediately write the exact expression of the Green's function on a Bethe lattice using the previous general expression (16):

$$G(R_n, \bar{\omega}) = \Omega(R_n) G^{Free}(\bar{\omega}) \quad (20)$$

where $G^{Free} = G_{BR}(\bar{\omega}) K(\bar{\omega})^n$. It is interesting that the “strong correlation” in the one hole problem in the Bethe lattice is only contained in the static function $\Omega(R_n)$, since $G^{Free}(\omega)$ is exactly the free electron Green's function. This has direct consequences on the spin charge decoupling. (See next section)

2. $t - J_z$: Brinkman-Rice Almost “Exact”

Let us consider the diagonal Green's function $G(R = O, \omega)$ for the $t - J_z$ model. In the general expression (16), $\Omega(\{R_l\}^n)$ is either one or zero depending on whether a given

permutation preserves the Néel order or not. The shortest skeleton paths with $\Omega(\{R_l\}^n) = 1$ is known to be three times the path around the elementary square plaquette. Thus $n = 12$ for such a skeleton path. There are 8 possibilities to build such a path starting from the origin in 2D (4 neighbors times 2 possible opposite directions) and $2d(2d - 2)$ in dimension d . Then the next leading correction to the Brinkman and Rice result is

$$G(R = O, \omega) = G_{BR}(\omega) \left(1 + 2d(2d - 2) K(\omega)^{12} + \dots \right) \quad (21)$$

Since $|K(\omega)| \leq \frac{1}{\sqrt{2d-1}}$ for any ω , the correction to the Brinkman and Rice result turns out to be less than 1.1% in $d = 2$ and 0.15% in $d = 3$. This has also been noted in $\frac{1}{d}$ expansion [10] but appears also quite natural in this formalism.

C. Spin Charge Decoupling

In 1D, if spin charge decoupling occurs, the one particle Green's function can be written as a simple product of a spinon contribution and a holon contribution:

$$G(R, t) = G^{spinon}(R, t) G^{holon}(R, t) \quad (22)$$

This property is exact in $d = 1$ for the infinite U Hubbard model and is asymptotically valid for large (R, t) at finite U . [21]

The spin charge decoupling manifests itself in the one particle Green's function and in principle can be detected even at higher dimensionality as speculated by several authors following P.W. Anderson. [2] For $J, J_z \rightarrow 0$, or $U \rightarrow \infty$ one expects no dynamics for the spinons and that the holon contribution has exactly the free particle behavior, because there is only a unitary charge carried by the single hole.

Thus, as a consequence of spin charge separation, the one hole Green's function should be written in the following way:

$$G(R, t) = \Omega(R) G^{Free}(R, t) \quad (23)$$

The free electron Green's function is nothing but the free propagator in the Nagaoka limit:

$$G^{Free}(k, \omega) = \frac{1}{\omega - \epsilon_k + i\delta \text{sgn } \omega} \quad (24)$$

where $\epsilon_k = 2t(\cos k_x + \cos k_y)$ is the energy of a free hole.

By Fourier transforming in time and by taking the imaginary part of the equation (23) we obtain the spectral weight as a function of the final position of the hole and the frequency ω :

$$A(\omega, R) = \Omega(R) A^{Free}(\omega, R) \quad (25)$$

The previous expression is exact in one dimension even for this simplified $t - J_z$ model where the spinon function is particularly simple $\Omega(R) = \delta_{R,O}$. [21] By Eq. (20) spin-charge decoupling is valid in the Bethe lattice for the single hole problem.

Equation (25) can be considered as a direct and measurable consequence of spin-charge separation. In fact, by measuring the spectral weight for two different positions of the hole we should get that the ratio:

$$\frac{A(\omega, R')}{A(\omega, R)} = \frac{\Omega(R')}{\Omega(R)} = \text{independent of } \omega \quad (26)$$

The ratio $\frac{A(\omega, R')}{A(\omega, R)}$, according to expression (26), should be independent of ω if spin-charge decoupling occurs. This is unlikely in dimension higher than one as the presence of the skeleton paths strongly renormalizes the spectral weight with the distance of the hole from the origin. [22] The absence of spin-charge decoupling is particularly evident already for the 2C case (Fig.1), where $A(\omega, R)/A(\omega, R = O)$ is ω dependent for relatively large R and quite low energy.

Based on the numerical and the analytical results, we conclude that spin-charge decoupling can occur mainly in lattices where closed loop paths are forbidden by the geometry. In these type of lattices the Nagaoka theorem cannot be applied. We have thus found an interesting relation between the Nagaoka theorem, spin charge decoupling and presence or absence of skeleton paths in a given lattice. Of course we cannot rule out more complicated form of spin-charge decoupling such as the one discussed in [23], or that at finite doping the situation may change. [17]

III. LANCZOS SCHEME

The Lanczos technique is widely used in strongly correlated electron systems. Contrary to the quantum Monte Carlo technique, it does not suffer the “fermion sign problem” or any other instabilities at low temperature. Dynamical correlations can be easily obtained using this technique. However, it has been restricted so far to small systems, typically 4×4 (for Hubbard models), or at most 26 sites (for t - J and t - J_z models) and 36 sites (for Heisenberg models). [14] On the other hand a systematic way for a finite-size scaling analysis in doped system such as the t - J_z model is not known yet and some infinite-system properties are still unclear or even misleading.

In this section, we will develop a scheme, which allows us to analyze the infinite system Lanczos data in a very efficient way, so that we are able to calculate the spectral function of the t - J_z model with good accuracy.

The Lanczos method is devised to diagonalize huge Hamiltonian matrix with dimension N_h . The method starts with a trial wave function ϕ_T . A new basis is generated by Hamiltonian multiplication,

$$\mathbf{s}_i = H^i |\phi_T\rangle \quad \text{for } i = 0, 1, \dots, n \quad (27)$$

Then an orthogonal basis $\{\mathbf{e}_i\}$ can be iteratively calculated, after orthogonalization of the vectors \mathbf{s}_i . Formally we have

$$\begin{aligned} b_{i+1} |e_{i+1}\rangle &= H |e_i\rangle - a_i |e_i\rangle - b_i |e_{i-1}\rangle \\ a_i &= \langle e_i | H | e_i \rangle \\ b_{i+1} &= \langle e_{i+1} | H | e_i \rangle \end{aligned} \quad (28)$$

where $b_0 = 0$, $|e_0\rangle = |\phi_T\rangle$. In the Lanczos basis, the Hamiltonian turns to a tridiagonal form where a_i are the diagonal elements and b_i the off-diagonal ones for $i = 1, \dots, n$.

For $n = N_h$, the spectrum of the tridiagonal matrix coincides with the one of the original Hamiltonian. Unfortunately the dimension of the Hilbert space is usually given by $N_h \sim$

$10^7 \div 10^9$, and it is prohibitive to perform a full diagonalization with the available computers. Nevertheless the ground state and the corresponding energy converge for relatively small $n \sim 10^2 \ll N_h$. This justifies the success of the method which enables to restrict the diagonalization to a very small basis $n \ll N_h$ where, according to the Ritz theorem, the variational principle applies for all the eigenvalues of the smaller tridiagonal matrix and in particular for the ground state energy.

A. Lanczos scheme in an Infinite Lattice

In an infinite system, the Lanczos scheme (28) can be applied efficiently, provided there is a proper way to define a simple *finite* basis to represent the vectors $s_n = H^n |\psi_T\rangle$ (27), generated by the iterative application of H to the trial state. This is in fact the case for the effective t - J_z Hamiltonian (13), where \mathbf{s}_i is represented by overturned spins on the Néel state localized around the hole.

For any fixed momentum p , we start from a Néel state with a hole at origin. Since the J_z term of the Hamiltonian is diagonal, the only part of the effective t - J_z Hamiltonian, relevant to generate new states, is the kinetic term. In each multiplication of the effective Hamiltonian, the hole is translated to its z nearest neighbors by the translation operator T_{τ_μ} (see Fig.(2)). Then the spin exchange operators χ_{O,τ_μ} move the hole back to the origin, leaving an overturned spin background and generating z new states.

The possibility to work with a finite basis even in the infinite system was first noted by Trugman [8]. In fact the overturned spins are located within a region around the hole with radius n . We can thus update only the defects over the Néel state, which are finite at any finite number of multiplications of H . After n steps, the Hilbert space is finite having at most dimension z^n .

This exponential growth of the Hilbert space $\sim z^n$ makes the problem intractable even for relatively small n . Fortunately many of the generated states appear several times during the expansion of the Hilbert space, due to the presence of the Trugman-like paths, [8] and

also due to the translation symmetry implicitly exploited by use of the effective Hamiltonian (13). After all, the dimension of the Hilbert space turns out to be considerably smaller than the previous estimate, and in fact it grows much slower than z^n , e.g. $\sim 1.9^n$ for $z = 3$. In this way we have reached $n = 26$ for the 2C case and $n = 14$ for the 2D case with an Hilbert space dimension at most equal to $\sim 12.2 \times 10^6$.

The *smallest* finite lattice which contains the full information of the first exact n Lanczos steps has linear dimension $2n + 1$. Therefore, our results correspond to a 53×2 lattice in the 2C case and to a 27×27 in 2D, which is by far larger than the size of a typical finite size Lanczos calculation [14]. However the finiteness of n often leads to appreciable systematic errors. In these cases we overcome this difficulty by carrying out a systematic extrapolation in $1/n \rightarrow 0$, following a scheme which is analogous to the finite size scaling analysis for finite lattice calculations.

We conclude this section with some technical comments about the algorithm. The basis generated by the iterative application of H_p^{eff} does not depend on the momentum p of the hole. Hence we only need to generate it once, which takes less than two hundred seconds of CPU time on a Cray-C90. After that, we can do the usual Lanczos iterations for fixed parameters p and J_z , which typically takes $10^2 \div 10^3$ seconds of CPU time on the same computer.

B. Lanczos Spectra Decoding

With the $n + 1$ eigenvalues E_i and eigenfunction $|\Psi_i\rangle$ of the Lanczos matrix truncated after n step, the spectral weight can be formally calculated as

$$\begin{aligned} A(k, \omega) &= \text{Im} \frac{1}{\pi} \langle \Psi_T | \frac{1}{\omega - H - i\delta} | \Psi_T \rangle \\ &= \sum_{i=0}^n |\langle \Psi_i | \Psi_T \rangle|^2 \delta(\omega - E_i) \end{aligned} \tag{29}$$

In the following we assume that the energies E_i are set in ascending order : $E_{i+1} > E_i$.

As a result of the finiteness of the restricted Hilbert space, we get a sum of δ -functions in the spectral weight at any fixed n . Due to the Lehmann representation of the spectral

function [24] this feature is also present in any finite size calculation. In this case the thermodynamic limit is obtained by smoothing the δ -functions in Eq. (29) with Lorentzians of a given small width δ , [14,15]

$$\delta(\omega - E_i) \rightarrow \text{Im} \frac{\pi^{-1}}{\omega - E_i - i\delta} \quad (30)$$

and then taking the limit $\delta \rightarrow 0$. For small finite δ , reasonable results can be obtained by the finite size Lanczos algorithm, provided that the resolution of the energy levels becomes much smaller than δ , i.e. n large enough but still much less than N_h . [14]

Numerically we have been able to perform $n = 26$ and $n = 14$ Lanczos iterations for the 2C and the 2D lattice respectively. Even though the ground state energy is already well convergent, such a small number of Lanczos steps is usually far from enough for a good estimate of the spectral weight. In fact by the conventional method of smoothing the δ -functions described in (30), either one miss the details of the spectral weight for large δ or in the opposite case one gets too rapid oscillations which are obviously unphysical. [25]

A more efficient method for evaluating the spectral weight was recently introduced by us. [25] In the following, for reason of completeness we will give a brief review of this new method named Lanczos Spectra Decoding. In this simple method, we introduced an interpretation of the Lanczos scheme. With this interpretation, the spectral function can be calculated accurately, efficiently and easily even with a small number of iterations n . As we have seen in fact the Lanczos scheme in the infinite system has a computational cost growing exponentially with n , whereas in any finite size calculation the algorithm is only linear in n . We expect therefore that our method is essential in the first case but maybe helpful only for a small computer-time factor in a finite size calculation.

As well known the spectral weight $A(\omega)$ is a distribution that may be divided into two parts $A(\omega) = A_{coh}(\omega) + A_{incoh}(\omega)$, a coherent one $A_{coh}(\omega)$ which contains only δ -function contributions and an incoherent one $A_{incoh}(\omega)$ which is a continuous and usually smooth function of ω . The Lanczos spectra decoding exploits the smoothness properties of $A_{incoh}(\omega)$ in a simple and efficient way. In the following we therefore assume that the spectral weight

is incoherent. This is not a limitation since coherent peaks can be easily separated out from the incoherent part by identifying all the quasiparticle weights $Z_i = |\langle \Psi_i | \Psi_T \rangle|^2$ that remain finite for $n \rightarrow \infty$.

If the spectral weight is incoherent, since by completeness $\sum_{i=0}^n Z_i = 1$, one expects that $Z_i \propto \frac{1}{n}$. Thus

$$Z(\omega) = (n+1)Z_i \quad (31)$$

may define a smooth function of ω at the discrete Lanczos energies $\omega = E_i$. The full spectral weight is then closely related to the previous function:

$$A(\omega) = Z(\omega)\rho_L(\omega) \quad (32)$$

where ρ_L represents the Lanczos density of states (LDOS) in the restricted Hilbert space generated by the Lanczos algorithm:

$$\rho_L(\omega) = \frac{1}{n+1} \sum_{i=0}^n \delta(\omega - E_i) \quad (33)$$

where the factor $\frac{1}{n+1}$ is determined by the normalization condition $\int_{-\infty}^{\infty} d\epsilon \rho_L(\epsilon) = 1$. For $n = N_h$ in a finite system, ρ_L coincides with the actual density of states of the many body system, but, in an infinite lattice ($N_h = \infty$), this is not generally true, as it will be shown for the Bethe lattice case.

By definition, the number of states dN between energies ϵ and $\epsilon + d\epsilon$ is given by

$$dN = (n+1)\rho_L(\epsilon)d\epsilon. \quad (34)$$

So the Lanczos density of states can be calculated as

$$\rho_L(\epsilon) = \frac{1}{n+1} \frac{dN}{d\epsilon} \quad (35)$$

Finally, using finite difference instead of differential, the coarse grained Lanczos density of states can be estimated up to order $O(\frac{1}{n^2})$ by

$$\rho_L(\bar{\epsilon}_i) = \frac{1}{(n+1)(E_{i+1} - E_i)}, \quad (36)$$

where the energies

$$\bar{\epsilon}_i = \frac{E_i + E_{i+1}}{2} \quad (37)$$

lie at the middle of two consecutive eigenvalues.

The function $Z(\omega)$ which is known at energies E_i can be easily interpolated at the energies $\bar{\epsilon}_i$ where also ρ_L is known:

$$Z(\bar{\epsilon}_i) = (Z_{i+1} + Z_i)/2. \quad (38)$$

If $Z(\omega)$ is a twice-differentiable function, eq. (38) is accurate up to $O(\frac{1}{n^2})$ as well. Thus within the same accuracy $A(\omega) = Z(\omega)\rho_L(\omega)$ easily follows at the discrete energies $\omega = \bar{\epsilon}_i$:

$$A(\bar{\epsilon}_i) = \frac{1}{2} \left(\frac{Z_{i+1} + Z_i}{E_{i+1} - E_i} \right). \quad (39)$$

The knowledge of $A(\omega)$ close to the previous “special” points $\bar{\epsilon}_i$ can be easily achieved by standard piecewise interpolations or extrapolations. At the end, we can verify the sum rule $\int A(\omega)d\omega = 1$, as a check for the accuracy of the calculation.

IV. LANCZOS SPECTRA DECODING ON THE BETHE LATTICE

In this section we will show that $Z(\omega)$ and $\rho_L(\omega)$ are well defined functions and can be calculated exactly in the Bethe lattice.

On the Bethe lattice, the problem is exactly solvable because the skeleton paths are absent and the retraceable paths can be summed analytically. This exact solution has two meaning for us: (1) as a test for our scheme and assumptions, (2) as an hint to interpret the Lanczos scheme for the physical 2C and 2D lattices.

Using the Lanczos basis defined in Eq.(28), the Hamiltonian has vanishing diagonal part ($a_n = 0$) and

$$\begin{aligned} b_1 &= \sqrt{z} \\ b_n &= \sqrt{z-1} \quad \text{for } n > 1 \end{aligned} \quad (40)$$

This easily follows since, on the Bethe lattice, each multiplication of the Hamiltonian generates $z - 1$ new states, except for the first iteration, which generates z states. Due to the simplicity of such Lanczos matrix it is then possible to compute analytically Z and ρ_L in eqs.(31,33).

In fact the wavefunction components ψ_i , $i = 0, 1, \dots, n$ of an eigenstate with energy ω satisfy the iterative relation in the Lanczos basis:

$$\begin{aligned}\sqrt{z}\psi_1 &= \omega\psi_0 & i = 0 \\ \sqrt{z}\psi_0 + \sqrt{z-1}\psi_2 &= \omega\psi_1 & i = 1 \\ (\psi_{i+1} + \psi_{i-1})\sqrt{z-1} &= \omega\psi_i & i \geq 2\end{aligned}$$

From the third equation solutions are possible for $\omega^2 < \epsilon_{BR}^2$ where $\epsilon_{BR} = -2t\sqrt{z-1}$ is the Brinkman-Rice approximation for the single hole ground state energy. Then the components of the eigenstates on the Lanczos basis are given by: $\psi_i = \text{Re} \left(A \lambda^i - 1 \right)$, where $\lambda = \frac{\sqrt{\omega^2 - \epsilon_{BR}^2} - \omega}{\epsilon_{BR}}$ and the complex number A is obtained by the first two equations, yielding $\psi_1 = \frac{\omega}{\sqrt{z}} \psi_0$ and $\psi_2 = \frac{\omega^2 - z}{\sqrt{z(z-1)}} \psi_0$. Finally ψ_0 is determined by the normalization condition $\sum_i \psi_i^2 = 1$, and the function $Z(\omega) = \lim_{n \rightarrow \infty} \psi_0^2(n+1)$ reads:

$$Z(\omega) = \frac{z^2 t^2 [\epsilon_{BR}^2 - \omega^2]}{2[z^4 t^4 - (2z+1)t^2 \omega^2]} \quad \text{for } \omega^2 < \epsilon_{BR}^2 \quad (41)$$

The Lanczos density of states (33) is then determined by:

$$\rho_L(\omega) = A(\omega)/Z(\omega) \quad (42)$$

where $A(\omega)$ is the Bethe lattice density of states in Eq.(4). In this case, $\rho_L(\omega)$ has singular inverse square root behavior near the band tail.

By use of the Lanczos Spectra decoding introduced in the previous section we have obtained a good approximation to the exact solution with $n \sim 10$, much less than in the conventional calculation. [25]

At finite J_z , the only change is with the diagonal part of the Lanczos matrix

$$a_0 = \frac{J_z}{4}z \quad (43)$$

$$a_i = \frac{J_z}{4}(3z - 1 + 2(z - 2)(i - 1)) \quad \text{for } i \neq 0 \quad (44)$$

This result can be easily obtained by counting the number of broken bonds in the states generated at different Lanczos iterations. In this formalism we obtain therefore that the motion of a hole in a Bethe lattice is exactly equivalent to a one dimensional motion of a particle in a linear potential, provided we identify the distance of the particle from the origin with the label i of the Lanczos basis.

By diagonalizing numerically the Lanczos matrix for large n we can easily confirm the prediction of the long wavelength hamiltonian (5), namely that the spectral function is k -independent, and that $A(\omega)$ contains only δ -function peaks. In fact due to the linear potential *all* of the one-hole states are localized states. It is important to remark that the corrections to the asymptotic $J_z \rightarrow 0$ behavior is quite important for the quasiparticle weight Z even for very small J_z . For Z the correct linear behavior $\propto J_z$ is found only for $J_z \sim 10^{-3}$ (see Fig.(3)), whereas the behavior of the ground state energy and the gap are more reasonable.

V. RESULTS AND DISCUSSION

A. Spectral weight for the $J_z = 0$ case

For $J_z = 0$ the spectral weight $A(\omega)$ is an even function of ω and in the following we will concentrate on its negative frequency region. In this model we found [25] a sharp peak in the spectral weight located at an energy close to the retraceable path prediction, $\epsilon_{BR} = -2t\sqrt{z-1}$, and, a second peak at energy $\sim -t$. In the 2D case, the spectral weight looks similar, although the first peak is rather small. In 1D, the exact BR solution leads only to one peak but with a divergent spectral weight $\sim \frac{1}{\sqrt{\omega-\epsilon_B}}$ at the bottom ϵ_B of the band. Already in the 2C case such a divergence disappears within the retraceable path approximation, as well as in our numerical scheme, which includes all closed-loop paths.

We also found that the first peak in the spectral function has a remarkable dispersive feature although the bottom of the spectrum appears k -independent. The dispersion of the first peak is not present neither in 1D or in infinite dimension [10] and the importance to go beyond the retraceable path approximation is already clear even in 2D.

For the density of states $D(\omega) = \int \frac{dp^d}{(2\pi)^d} A(\omega, p) = A(R = O, \omega)$, our results present some small oscillations around the retraceable path analytic solution (3). In 2D however the retraceable path expression for $z = 4$ seems already quite accurate, at least away from the band tails. [25] All the above results have been confirmed recently . [20]

As discussed in the introduction a key question is the determination of the band edge energy ϵ_B , i.e. the threshold energy where the spectral weight begin to vanish. As a first step we identify the Lanczos ground state energy E_n for $n \rightarrow \infty$ as ϵ_B , which may or may not converge to the Nagaoka energy ϵ_N . For instance, by neglecting closed loop paths, one obtains the Brinkman-Rice energy ϵ_{BR} as a variational estimate of E_∞ . In the retraceable path approximation ϵ_B coincides with E_∞ , as one generally expects.

In order to have an accurate estimate of E_∞ , it is useful to have a guess about the asymptotic behavior of the quantity $\Delta_n = E_n - E_\infty$ for $n \rightarrow \infty$. The way Δ_n vanishes for $n \rightarrow \infty$ is related to the form of the Lanczos density of states at low energy. In the Brinkman-Rice case the exact solution in (4) gives $\rho_L(\epsilon) \sim (\omega - \epsilon_B)^{-1/2}$. Thus, using Eqs. (36), $\Delta_n^{-1/2} \sim \frac{1}{n\Delta_n}$, yielding $\Delta_n \sim \frac{1}{n^2}$. For $J_z = 0$ the inclusion of the skeleton paths seems to support a finite Lanczos density of states (see Fig.(4)), yielding, by the same argument $\Delta_n \sim \frac{1}{n}$. We have plotted in Fig.(5) the estimated ground state energies as a function of $1/n$ for several momenta for the 2D and the 2C cases. Many of the estimated Lanczos energies – exact upper bound of the true ground state energy– are clearly below ϵ_{BR} (even for the 2D case also shown in the picture). Thus, a previous suggestion that the one hole energy in a quantum antiferromagnet should be close to ϵ_{BR} [26,27] *is not confirmed* by our numerical results. In Fig.(5) -2C case- it is remarkable that all of the extrapolated energies are very close to the Nagaoka energy, independent of the momentum of the hole, i.e. $E_\infty = -3 \pm 0.02$.

The above results give a robust evidence that ρ_{LDOS} is finite up to the Nagaoka energy. Even in this case the spectral weight $A(\omega) = Z(\omega)\rho_{LDOS}(\omega)$ can in principle vanish for $\omega > \epsilon_N$ due to the vanishing of the factor $Z(\omega)$. This is the scenario suggested in [20] using the expansion for the Green's function in terms of $K(\omega)$ (16). In the interval $K(\omega)\alpha < 1$ (for $|\omega|/t > \frac{(z-1)}{\alpha} + \alpha$) when the expansion (16) converges the Green's function is surely real, thus determining a lower bound for ϵ_B . After some extrapolation it was found in [20] that $\alpha < z - 1$, i.e. ϵ_B should be higher than ϵ_N for the 2C or the 2D case using the first 18 or 12 coefficients $C_n(R)$ of the Green's function expansion, respectively. Although the above analysis is surely correct, the basic conclusion is affected by systematic errors due to the limited knowledge of a few coefficients in the expansion.

As it is shown in Fig.6, this scenario looks unlikely within the Lanczos Spectra decoding method because $Z(\omega)$ seems to be smoothly connected to the Nagaoka energy. It is clear however that this is not enough for a definite conclusion.

In order to solve the latter controversy without relying on the Lanczos spectra decoding, we have reproduced the Müller-Hartmann–Ventura expansion (Table I) and extended it up to the first 26 coefficients for the 2C case. Since we have generated all of the \mathbf{s}_i , defined in (27), up to $i = n = 26$ for the 2C case, the total number of paths of length $2n$ can be easily calculated as

$$M_n = \langle \mathbf{s}_n | \mathbf{s}_n \rangle \quad (45)$$

By proper undressing the retraceable paths, we can convert the total number of paths M_n to the number of the skeleton paths C_n .

As it is shown in table I the Müller-Hartmann–Ventura extrapolation:

$$C_n(R) = C(R) \frac{\alpha^{2n}}{(2n)^{\beta(R)}} \quad (46)$$

used to determine the radius of convergence α is not stable when large skeleton paths are included. For large n , we find that α , $\beta(R = O)$ and $C(R = O)$ are always going up. At $n = 26$, $C(R = O)$ becomes 10 times larger than their value obtained for $n = 18$, while α changes from 1.88 to 1.91. (Table I)

Instead of using the fit (46), we apply the well established ratio method, which is well known in the study of critical phenomena. Using this method we evaluate the radius of convergence α , and the power law exponent θ describing the vanishing of the Green's function at the band tails, corresponding to the critical temperature and to the conventional critical exponent in the language of critical phenomena, respectively. [28] We define

$$\mu(n) = \sqrt{\frac{C_n}{C_{n-1}}} \quad (47)$$

and the linear intercept at $\frac{1}{n} \rightarrow 0$ with two next consecutive points

$$\mu(n, n-2) = \frac{1}{2}[n\mu(n) - (n-2)\mu(n-2)]. \quad (48)$$

In fact μ is expected to behave as

$$\mu(n) = \alpha[1 + \frac{g}{n} + O(\frac{1}{n^2})] \quad (49)$$

where α gives the position of the singularity and $\theta = -(1+g)$ gives the exponent of the Green's function at the band tail $G(\omega) \propto (\omega - \epsilon_B)^\theta$. This kind of analysis is much more stable than the extrapolation used in [20]. In Fig.(7) the data for the linear intercept $\mu(n, n-2)$ suggests that the $\frac{1}{n}$ corrections are well behaved, and approximately linear for $n > 20$. By accident this number is very close to the maximum n available in the previous analysis [20], giving further evidence that for this problem a very large number of coefficients C_n are necessary to obtain reasonably converged results.

Then, by a linear fit in the region $n > 20$, we obtain $\alpha = z - 1$ within one per cent, both for $R = 0$ and for $p = 0$, as an independent check that α should not depend on R ($C_n(p=0) = \sum_R C_n(R)$). This is a clear evidence that the band edge energy coincides with the Nagaoka energy.

For the 2D case the data shown in Fig. (8) indicate that the above analysis is poorly converged due to a too much small value of $n = 14$. This also explains why the extrapolated $n \rightarrow \infty$ results for E_∞ , shown in Fig(5), does not converge to ϵ_N in 2D.

For the critical exponent θ we have a much less accurate result probably because the vanishing of the spectral weight close to ϵ_N is characterized by overall essential singularities of the type $e^{-\frac{1}{\omega-\epsilon_N}}$, as we have suggested in our previous paper. [25]

Here we can give a very simple argument supporting the expected singular behavior for $Z(\omega)$. For the spectral weight the behavior close to ϵ_N should be the same, because, as we have previously shown, the Lanczos density of states is approximately constant in this region.

After n Lanczos steps the hole forms a polaron state $|P\rangle$ with maximum spin but total $S_z = 0$ [29] in a region of linear size $\xi \sim n$, as it is also confirmed by direct calculation of the spin arrangement around the hole (see next section). The overlap of the Néel state and this trial state is then approximately given by [29]:

$$Z_0 \sim \frac{1}{\binom{V}{V/2}} \rightarrow \sqrt{\frac{\pi V}{2}} 2^{-V} \quad (50)$$

where V is the volume of the polaron equal to 2ξ for the 2C case and $\propto \xi^d$ for general spatial dimension $d > 1$. The quantity $Z_0 \times n$ according to the Lanczos spectra decoding method characterizes the behavior of the smooth function $Z(\omega)$ at an energy $\omega = \epsilon_N + \text{const.}/n$. Solving for n from the latter equation and assuming, as we have already mentioned, that $\xi \propto n$ we can substitute $V \propto (\omega - \epsilon_B)^{-d}$ in (50) and obtain:

$$A(\omega) \propto Z(\omega) \propto (\omega - \epsilon_N)^{-3/2} e^{-\frac{\Delta}{(\omega-\epsilon_N)}} \quad \text{for 2C} \quad (51)$$

$$A(\omega) \propto Z(\omega) \propto (\omega - \epsilon_N)^{-d/2-1} e^{-\frac{\Delta}{(\omega-\epsilon_N)^d}} \quad \text{for } d > 1 \quad (52)$$

where Δ is an overall constant depending on the dimensionality. Using the above formulas we have obtained good agreement with numerical results over a range for Z covering up to two decades (see Fig.(9)).

B. Spectral weight for finite J_z

For finite J_z a coherent part shows up in the spectral weight. However, contrary to the string picture, only the first few energy levels contribute to the spectral weight with true

δ - functions (See Fig.(10)). In order to identify these δ - function contributions we can check whether the quasiparticle weight Z_i converge to some *finite* value for $n \rightarrow \infty$, whereas if the energy level E_i belongs to the incoherent part $Z(\omega) = (n + 1)Z_i$ remains finite for $n \rightarrow \infty$. Another method to distinguish the coherent part from the incoherent one is to analyze directly the wavefunction components of the eigenstate Ψ_i on the Lanczos basis $\{e_j\}$. As we have seen in the previous section the label j measures the length of the overturned spins in the state i . The quasiparticle weights Z_i are finite only if the Néel state $e_{j=0}$ will have a non vanishing component with the state Ψ_i . This obviously occurs if the eigenstate Ψ_i is “localized” in the Lanczos basis even for $n \rightarrow \infty$, otherwise only a probability $\sim \frac{1}{n}$ to be in the Néel state is expected.

Using the above criteria, shown in Fig.(11), we have a clear evidence of a single quasiparticle weight for J_z not too large, and an incoherent part which is rather similar to the $J_z = 0$ one. For larger J_z the incoherent part moves quite fast to higher energies, leaving probably more than one δ -function contributions to the spectral weight. We then conclude that the inclusion of closed loop paths does not suppress the first quasiparticle weight, but completely washes out all the quasiparticle excitations at higher energies. Even the few peaks that appears in the incoherent part cannot be associated to “string state” resonances -as suggested by [15,30]- but are rather similar to the $J_z = 0$ ones, where localized string states cannot exist. We thus confirm the conclusions of Poilblanc. [14]

As far as the energy spectrum $E(p)$ is concerned we obviously found that the lowest energy state has a finite quasiparticle weight and has momentum $p = (0, 0)$, instead of $(\frac{\pi}{2}, \frac{\pi}{2})$ as commonly accepted for the t - J model. [31,9] This is because in the t - J_z model the spin fluctuations are neglected, while they play an important role for the energy dispersion $E(p)$.

Finally for the quasiparticle weight as a function of J_z we can apply the same argument at the end of the previous section by assuming that Z is basically the overlap of an $S_z = 0$ polaron state of size ξ , where ξ may be roughly identified as the correlation length within the string picture $\xi \propto J_z^{-1/3}$. We should get essential singularities like

$$\begin{aligned}
Z &\propto J_z^{-1/6} e^{-\Delta J_z^{-1/3}} \quad \text{for } 2C \\
Z &\propto J_z^{-d/6} e^{\frac{-\Delta}{J_z^{d/3}}} \quad \text{for } d > 1.
\end{aligned} \tag{53}$$

As in the string picture, where we could not detect the correct $Z \propto J_z$ behavior for reasonably small values of J_z (see Fig.(3)), we expect that these kind of singularities are important only at a value of $J_z \sim 10^{-3}$. For larger values of J_z one obtains a crossover to a $J_z^{2/3}$ behavior surprisingly valid for a quite large range of J_z both in the string picture and in the realistic cases shown in Fig.(3,12). In the latter picture it is also evident that at some small value of J_z the Z factor should vanish much faster than $J_z^{2/3}$, otherwise we should get an unplausible critical value of J_z , where the quasiparticle weight vanishes. This at least supports the behaviour for Z shown in Eq.(53).

C. Ground state properties for small J_z

The accurate determination of the ground state energy in the small J_z region is important to detect a possible transition between a uniform antiferromagnetic state and a state where the hole fully polarize the spins in a finite region of space with size ξ^d , region being somehow phase-separated from the remaining antiferromagnetic region. The latter variational state has an energy approaching the Nagaoka energy for $\xi \rightarrow \infty$. At finite J_z , by optimizing the size ξ of the ferromagnetic region, corrections to the asymptotic Nagaoka energy scale like $\frac{2}{J_z^{d+2}}$. [27]

Support for a possible transition comes from the infinite dimension limit [10]. In fact the exact evaluation of the Green's function, possible in infinite dimension, implies that the lowest energy state contributing to the spectral weight is analytically connected at small J_z not to the Nagaoka energy $\propto -d$ but to the much higher Brinkman-Rice energy $\propto -\sqrt{d}$. If the latter state is identified with the lowest energy state in a uniform antiferromagnetic phase, there should be a critical value J_c where the 'phase separated' state, discussed at the beginning of this section, becomes lower in energy for $J_z < J_c$. [27,15] This is essentially the

scenario proposed by Emery et al. for the doped $t - J$ model. We will show in the following a clear numerical evidence that the above scenario *is not confirmed* in the $t - J_z$ model for a single hole, at least in the 2C case.

Contrary to the string picture or the infinite dimension limit we see in Fig.(13) that the asymptotic value for the energy is clearly given by the Nagaoka energy, although the leading corrections to the energy seem quite well fitted by the string picture exponent $J_z^{2/3}$. In fact the diagonal elements of the Hamiltonian in the Lanczos basis describe approximately a linear potential (Fig.(14)) as in the string picture. This is obviously important for the small J_z correction to the energy. Moreover in Fig.(13) it is shown that the ‘phase separated’ state is well above the estimated energies even for very small J_z , leaving a possible transition at an unphysically small value of $J_z \sim 10^{-4}$ for the 2C case. For the 2D case however we do not have enough accuracy as shown in Fig.(8) and we cannot exclude a transition at $J_z \sim 10^{-2}t$.

D. Spin arrangement in the ground state

Although we have found evidence that the Nagaoka energy is the ground state energy of the $t - J_z$ model for $J_z \rightarrow 0$ it is not clear what spin background is favoured in this limit. For instance we could have that the Nagaoka state is degenerate in the thermodynamic limit with an antiferromagnetic state.

In order to solve this issue, we have calculated the hole-spin-spin correlation function, by measuring the one involving the spins in the z -direction

$$\begin{aligned} C_z^\mu(R_i) &= N \langle \psi_p | h_o^\dagger S_{R_i}^z S_{R_i+\tau_\mu}^z | \psi_p \rangle \\ &= \langle S_O | S_{R_i}^z S_{R_i+\tau_\mu}^z | S_O \rangle \end{aligned} \quad (54)$$

and its spin rotation invariant version

$$\begin{aligned} C^\mu(R_i) &= N \langle \psi_p | h_o^\dagger \mathbf{S}_{R_i} \mathbf{S}_{R_i+\tau_\mu} | \psi_p \rangle \\ &= \langle S_O | \mathbf{S}_{R_i} \mathbf{S}_{R_i+\tau_\mu} | S_O \rangle \end{aligned} \quad (55)$$

where h_o^\dagger is the hole creation operator at origin. These correlation functions measure how the spin background is perturbed by the hole.

The symmetrized correlation function $C^\mu(R_i)$ has been introduced since, for $J_z \rightarrow 0$, the total spin is a well defined quantum number and the isotropic hole spin-spin correlation does not depend on the polarization of the total spin. Thus even in the $S_z = 0$ sector a polaron solution with maximum spin leads to a maximum $C(R_i) = \frac{1}{4}$, whereas $C_z^\mu(R) = 0$ for this polarized state since the contribution of the parallel spins are exactly cancelled by the one of the antiparallel spins (all these contributions have the same weight in the polaron solution [29]). In this way, we can unambiguously distinguish the ferromagnetic region with $C^\mu(R_i) > 0$ from the antiferromagnetic one with $C^\mu(R_i) < 0$. As shown in Fig. 15, we have found that for large J_z all the spins are antiferromagnetically correlated in the z direction since the two previous correlation functions are almost identical. There is a clear evidence of an antiferromagnetic correlation which approaches the asymptotic value $C(R) \rightarrow -1/4$ with a correlation length consistent with the one shown in Fig. (11).

For small J_z , as expected, the finite n corrections are important and tends erroneously to enhance the antiferromagnetism (see Fig. (16)). Instead by studying the behavior of $C(R)$ and $C_z(R)$ as a function of $1/n$ it is quite clear that the spins are strongly correlated in the $x-y$ plane and for $n \rightarrow \infty$ and $J_z = 0$, the hole-spin-spin correlations seem to approach the fully polarized values $C(R) = 1/4$ and $C_z(R) = 0$, presumably at any finite distance from the hole.

VI. CONCLUSION

In conclusion the physical picture of the one hole ground state in the $t - J_z$ model seems clear. As we decrease J_z , we approach the Nagaoka state with maximum spin and with total $S_z = 0$ (which is by the way a conserved quantity) due to the proliferation of closed loop paths that strongly enhance the ferromagnetic correlations around the hole in the $x-y$ plane. Thus there exists a ferromagnetic polaron with a length which diverges for $J_z \rightarrow 0$, but that is continuously connected to the antiferromagnetic length obtained at finite large J_z . In this way the polaron state is somehow similar to the phase separated variational

state [27], but we have to emphasize that in our approach the localized polaron conserves the translational symmetry because it is defined after the Galileo transformation (7) and consequently it is not “phase separated”. Moreover the total spin projection on the z -axis vanishes, as it is conserved locally by the effective Hamiltonian (13). The energy of this state is much smaller than the “phase separated” variational state and represents a more accurate picture of the single hole ground state in the $t - J_z$ model.

We have presented here a successful attempt to go beyond the retraceable path approximation and the string picture for the hole dynamics in an antiferromagnetic spin background. A new Lanczos-type of analysis of the Hamiltonian enabled us to get very accurate results for the 2C problem and qualitatively similar ones for the 2D case. At $J_z = 0$, a clear dispersion of the main incoherent peak of $A(k, \omega)$ both for the 2C and the 2D case was found. Contrary to the prediction of the large spatial dimension we found, at least for the 2C model, that the bottom of the incoherent band is dispersionless and coincides with the Nagaoka energy ϵ_N , *i.e.* the minimum possible energy by the Nagaoka theorem. This resolve a controversy recently proposed by Müller-Hartmann and Ventura. In fact, based on the Lanczos Spectra Decoding method, we have given an argument implying that $A(\omega) \propto (\omega - \epsilon_N)^{-d/2-1} e^{\frac{-\Delta}{(\omega - \epsilon_N)^d}}$ and if for instance $\Delta \propto (\epsilon_{BR} - \epsilon_N)^d$, we can easily understand why the infinite dimension limit gets no weight for $\omega < \epsilon_{BR}$. As the dimensionality is increased the tail of the spectral weight below the Brinkman-Rice energy vanishes exponentially, though remaining always finite up to the Nagaoka energy in any finite d .

For finite J_z , contrary to the string picture, we found only one coherent quasi-particle weight and an incoherent broad spectrum at higher energy. A second quasiparticle peak may appear in the spectral function but has always a very small weight. The possibility of a phase transition as a function of J_z is not compatible with our numerical results for the ground state energy, unless for very small coupling constant, and consequently, the Emery’s argument about the phase separation for small J is found unlikely in the $t - J_z$ model.

The spin charge decoupling for a single hole is surely not evident for short distance propagations. However, it still remains open whether the spin charge decoupling happens

asymptotically at large distance, although for the 2C case we have ruled out this possibility up to a distance of about 10 lattice spacings.

We gratefully acknowledge useful discussions with A. Parola, E. Tosatti and D. Poilblanc. This work has been supported by CNR under Progetto Finalizzato “Sistemi informatici e calcolo parallelo”.

APPENDIX: QUASIPARTICLE WEIGHT, GREEN’S FUNCTION AND CURRENT OPERATORS

An important quantity to characterize the dynamics of the single hole is the so called quasi-particle weight appearing as the residue of a simple pole in the one-hole dynamical Green’s function. This residue can be alternatively calculated [32] by means of the overlap of the ground state $|\psi_p\rangle$ of one hole with momentum p and the state $c_{p,\sigma}|H\rangle$, where $|H\rangle$ is the translation invariant ground state without holes:

$$Z_p = |\langle H|c_{p,\sigma}^\dagger|\psi_p\rangle|^2 = |\langle H|S_O\rangle|^2 \quad (\text{A1})$$

where we have explicitly used that $n_{\sigma,O}|S_O\rangle = |S_O\rangle$. For $t > 0$, *i.e.* positive time, the Green’s function is defined as

$$G(p, t) = -2i \langle H|c_{p,\sigma}^\dagger e^{-i(H-i\delta-E_0)t} c_{p,\sigma}|H\rangle \quad (\text{A2})$$

where E_0 is the corresponding energy of the state $|H\rangle$. Here the factor two comes from the requirement that $G(p, t \rightarrow 0^+) = -2 \langle H|n_{p,\sigma}|H\rangle = -i$. The normalized state $|\psi_p\rangle = \sqrt{2}c_{p,\sigma}|H\rangle$ is of the form (7), if we choose

$$S_O^H = \sqrt{2}n_{\sigma,O}|H\rangle. \quad (\text{A3})$$

Due to the correspondence of eigenstates between H_p^{eff} and H , we can expand $|S_O\rangle$ in terms of eigenstates of H_p^{eff} and easily check that the propagation of $|S_O\rangle$ with the effective Hamiltonian, $|S_O\rangle_t = e^{iH_p^{eff}t}|S_O\rangle$, corresponds exactly to the propagation of ψ_p with the exact $t - J_z$ Hamiltonian and

$$G(p, t) = -i \langle S_O^H | e^{-i(H_p^{eff} - i\delta)t} | S_O^H \rangle \quad (\text{A4})$$

Using that $|S_O^H \rangle = \sqrt{2} n_{i,\sigma} |H \rangle$, that the commutator $[H_p^{eff}, n_{\sigma,O}]$ vanishes and that G does not depend on σ , we get, after Fourier transform $G(p, \omega) = \int_0^\infty dt G(p, t) e^{i\omega t}$,

$$G(p, \omega) = \langle H | \frac{1}{\omega + i\delta - H_p^{eff}} | H \rangle. \quad (\text{A5})$$

Another important quantity is the current operator, which is useful when we calculate the transport properties. On a discrete lattice, it is defined as [6]:

$$j_\mu = \left[ie_0 t \sum_{R\sigma} c_{R\sigma}^\dagger c_{R+\tau_\mu\sigma} + h.c. \right] \quad (\text{A6})$$

where e_0 is the electron charge. The matrix elements of the current operator between two one-hole states with given momentum p define an effective current operator j_μ^{eff} acting on spin states only:

$$\langle \psi_p^{S'} | j_\mu | \psi_p^S \rangle = \langle S' | j_\mu^{eff} | S \rangle \quad (\text{A7})$$

Analogously to the calculation shown in Section II, the effective current operator can be written as

$$j_\mu^{eff} = [-ie_0 t e^{ip\tau_\mu} \chi_{O\tau_\mu} T_{\tau_\mu} + h.c.] \quad (\text{A8})$$

REFERENCES

- [1] J.G. Bednorz and K.A. Muller, Z. Phys. **B64**, 189 (1986)
- [2] P.W. Anderson, Science 235, 1196 (1987).
- [3] M.C. Gutzwiller, Phys. Rev. Lett. **10**, 159 (1963).
- [4] J. Hubbard, Proc. Roy. Soc. **A276**, 238 (1963).
- [5] J. Kanamori, Progr. Theor. Phys. **30**, 275 (1963).
- [6] F.C. Zhang and T.M. Rice, Phys. Rev. B **37**, 3759 (1988).
- [7] Y. Lu, Z.B. Su and Y.M. Li Chinese Journal of Physics **31**, 579 (1993) and reference therein.
- [8] S.A. Trugman, Phys. Rev. B **37**, 1597 (1988).
- [9] C.L. Kane, P.A. Lee and N. Read, Phys. Rev. B **39**, 6880 (1989), S. Schmitt-Rink, C. M. Varma, and A. E. Ruckenstein, Phys. Rev. Lett. **60**, 2793 (1988).
- [10] see e.g. D. Vollhardt in "Correlated Electron Systems" ed. V. J. Emery (World Scientific Singapore, 1993) and reference therein.
- [11] W.F. Brinkman and T.M. Rice, Phys. Rev. B **2**, 1324 (1970).
- [12] L.N. Buleavskii, E.L. Nagaev and D.I. Khomskii, Sov. Phys. JETP **27**, 638 (1968).
- [13] B.I. Shraiman and E.D. Siggia, Phys. Rev. Lett. **60**, 740 (1988).
- [14] D.Poilblanc H. J. Schulz and T. Ziman, Phys. Rev. B **47**, 3268 (1993), *ibidem* Phys. Rev. B **46** 6435 (1992).
- [15] E. Dagotto, R. Joynt, A. Moreo, S. Bacci and E. Gagliano Phys. Rev. B **41**, 9049 (1990).
- [16] P. Prelovšek, I. Sega and J. Bonca Phys. Rev. B **42** 10706 (1990) *ibidem* Phys. Rev. B **39**, 7074 (1989).

- [17] W. O. Putikka, R. I. Glenister , R. R. Singh and H. Tsumetsugu, Phys. Rev. Lett. **73**, 170 (1994).
- [18] M. Ogata , M. Luchini, S. Sorella and F. Assaad , Phys. Rev. Lett. **66**, 2388 (1991).
- [19] A. Parola unpublished, T. Xiang Phys. Rev. B **44**, 2276 (1992).
- [20] E. Müller-Hartmann and C.I. Ventura Phys. Rev. B **50**, 9235 (1994).
- [21] A. Parola and S. Sorella, *Phys. Rev. B* **45**, 13156 (1992); S. Sorella and A. Parola, *J. Phys. Cond. Mat.* **4** 3589 (1992).
- [22] S. Sorella and Q.F. Zhong in “Correlation Effects in Low -Dimensional Electron System” edited by A. Okiji and N. Kawakami, p.185, Springer-Verlag (1994).
- [23] M. Fabrizio and A. Parola Phys. Rev. Lett. **70**, 226 (1993).
- [24] See for instance: A. L. Fetter and J.D. Walecka *Quantum theory of Many Particle Physics*, McGraw–Hill (1971).
- [25] Q.F. Zhong, S. Sorella and A. Parola, Phys. Rev. B **49**, 6408 (1994)
- [26] Y. Hasegawa and D. Poilblanc, Phys. Rev. B **40**, 9035 (1989).
- [27] V.J. Emery, S.A. Kivelson and H.Q. Lin Phys. Rev. Lett. **64**, 475 (1990).
- [28] D.S. Gaunt and A.J. Guttmann in *Phase Transition and Critical Phenomena* Vol. 3, Academic Press Inc. (London) Ltd. (1974).
- [29] The state $\langle P|$ with maximum spin and $S_z = 0$ has the same overlap with all the possible states of the Hilbert space with $S_z = 0$, thus in particular $\langle P|N \rangle^2 = \frac{1}{\binom{V}{V/2}}$, where $V = \xi^d$ is the volume occupied by the polaron, and the binomial coefficient $\binom{V}{V/2}$ is the number of ways to put $V/2$ spin up and $V/2$ spin down in a region of V spins.
- [30] Z. Lin and E. Manusakis Phys. Rev. B **44**, 2414 (1991).
- [31] M.D. Johnson, C. Gros and K.J. von Szczepanski, Phys. Rev. B **43**, 11207 (1991).

[32] P. W. Anderson, Phys. Rev. Lett. **64**, 1839 (1990); **65**, 2306.

FIGURES

FIG. 1. (a):The ratio of the spectral weight at different sites for the two chain lattice. The spectral weight as a function of R was obtained by Fourier transforming $A(p, \omega)$ obtained by the standard Lanczos Spectra Decoding. Moreover since at fixed n , $A(R, \omega)$ is exactly zero for R large enough, only a finite number of momenta are necessary to implement *exactly* the mentioned Fourier transform (b):The calculated spectral weight for $R = O$. The solid line is got by summing the spectral weight for all momenta verifying the independent relation $A(R = O, \omega) = \int \frac{dp}{2\pi} A(p, \omega)$. The data points are calculated directly by the Lanczos Spectra Decoding using a trial state with a hole localized at the origin, *i.e.* without using the translation invariance.

FIG. 2. The application of the effective t Hamiltonian(12) on the trial state. (a):The Néel state with one hole. The hole is located at origin. (b):The state after the action of T_{τ_μ} . T_{τ_μ} translates the Néel state one lattice space along the direction μ . The hole moves to the nearest neighbor. (c):The final state. The spin exchange operator moves the hole back to the origin and leaves an over-turned spin defect in the Néel background.

FIG. 3. The single hole quasiparticle weight of the t - J_z model on the Bethe lattice with $z = 3$ and $z = 4$. The inset is an expansion of the small J_z region and the axes have been scaled by a factor 1000. The Lanczos matrix was truncated after $n = 40000$ Lanczos steps, by far enough to obtain convergent $n = \infty$ results even for very small J_z .

FIG. 4. The Lanczos density of states on the Bethe lattice (for $z = 3$ and $z = 4$), the 2C and the 2D lattice. Triangles, squares and circles correspond to the small, medium and large n calculation respectively. The continuous lines are the exact results for the Bethe lattice and guides to the eye for the 2C and 2D lattices

FIG. 5. Plot of the lowest eigenvalues of the 2C and 2D model as a function of $1/n$, the inverse of the Lanczos-iteration number. For the 2C case, the wavevector k ranges from $(0,0)$ (bottom) to $(\pi,0)$ (top) with nine equally spaced values. For the 2D case the k -path in the magnetic Brillouin zone is $\Gamma \rightarrow M \rightarrow X \rightarrow \Gamma$, where $\Gamma = (0,0)$ (bottom), $M = (\pi,0)$ (top) and $X = (\pi/2, \pi/2)$. The horizontal dashed lines denote the Brinkman-Rice ground state energies.

FIG. 6. The expected smooth quantity $Z(\omega) = (n+1) \times Z$ at $J_z = 0$ plotted as a function of the energy for different Lanczos iterations. The continuous line connects the $n = 26$ data. By comparing the data at different Lanczos iterations, $Z(\omega)$ seems to be non vanishing just above the Nagaoka energy $\epsilon_N = -3t$ for 2C. The insert is an expansion of the band edge.

FIG. 7. The linear intercept $\mu(n, n-2)$ defined in the text (48) as a function of $\frac{1}{n}$ for $p = (0,0)$ and $R = (0,0)$. The dashed lines are linear extrapolations of the last six points. The two horizontal arrows indicate the Brinkman-Rice and Müller-Hartman-Ventura estimates. The vertical arrow indicates the largest n analyzed in [20].

FIG. 8. Same as in Fig. (7) for the 2D case, the data are taken from [20].

FIG. 9. The behavior of $Z(\omega)$ at band tail for $p = (0,0)$ and $p = (\pi,0)$. The solid lines are the least square fit by expression (52).

FIG. 10. The spectral function at $J_z = 0.3t$ and $k = (\pi,0)$ and $J_z = 2t$ and $k = (0,0)$. Z_1 and Z_2 are the quasiparticle weights for the lowest two eigenstates. The small value of Z_2 compared to Z_1 indicates that only the lowest weight remains finite for $n \rightarrow \infty$, i.e. contributing to the spectral weight with a true δ -function.

FIG. 11. The 2C-wavefunction of the single hole in the Lanczos basis for $J_z = 2t$, $p = (0,0)$ and $J_z = 0.3t$, $p = (\pi,0)$. The solid line denotes the ground state, the dotted one the first excited state and the dashed one the second excited state.

FIG. 12. Calculated quasiparticle weight Z as a function of $(J_z/t)^{2/3}$.

FIG. 13. The ground state energy as a function of $J_z^{2/3}$. The data points refers to $n = 26$ (2C) and $n = 14$ (2D). The continuous lines are a fit $E = a + bJ_z^{2/3} + cJ_z$ of the data. The dotted line is the energy of the “phase separated polaron” described in the text.

FIG. 14. The diagonal matrix elements of the Hamiltonian in the Lanczos basis. The solid line refers to the two-chain lattice and the dashed line to the corresponding Bethe lattice with $z = 3$.

FIG. 15. The hole spin-spin correlation function $C^\mu(R)$ and $C_z^\mu(R)$ with $\tau_\mu = (1, 0)$. For large J_z $C(R)$ is purely antiferromagnetic. However for vanishing (or small) J_z , the ferromagnetic component in the $x - y$ plane is important.

FIG. 16. The extrapolation $n \rightarrow \infty$ of $C^\mu(R)$ and $C_z^\mu(R)$ for the three lattice sites closest to the hole at $J_z = 0$. The horizontal line is the value of $C^\mu(R)$ for the fully polarized Nagaoka state.

TABLES

TABLE I. The non vanishing coefficients $C_n(R)$ of the t - J_z Hamiltonian on the 2C lattice. Only those coefficients which are not included in the Müller-Hartmanni-Ventura's table are shown. The notation is similar to the one in ref. [20], i.e. $d^2 = |R|^2$ and n_{d^2} is the number of skeleton paths at a given distance and for a given direction (note that there is an extra factor two for $R \neq O$ if we do not distinguish the two possible directions as in ref. [20]). The data for $n = 26$ are accurate up to ± 5 .

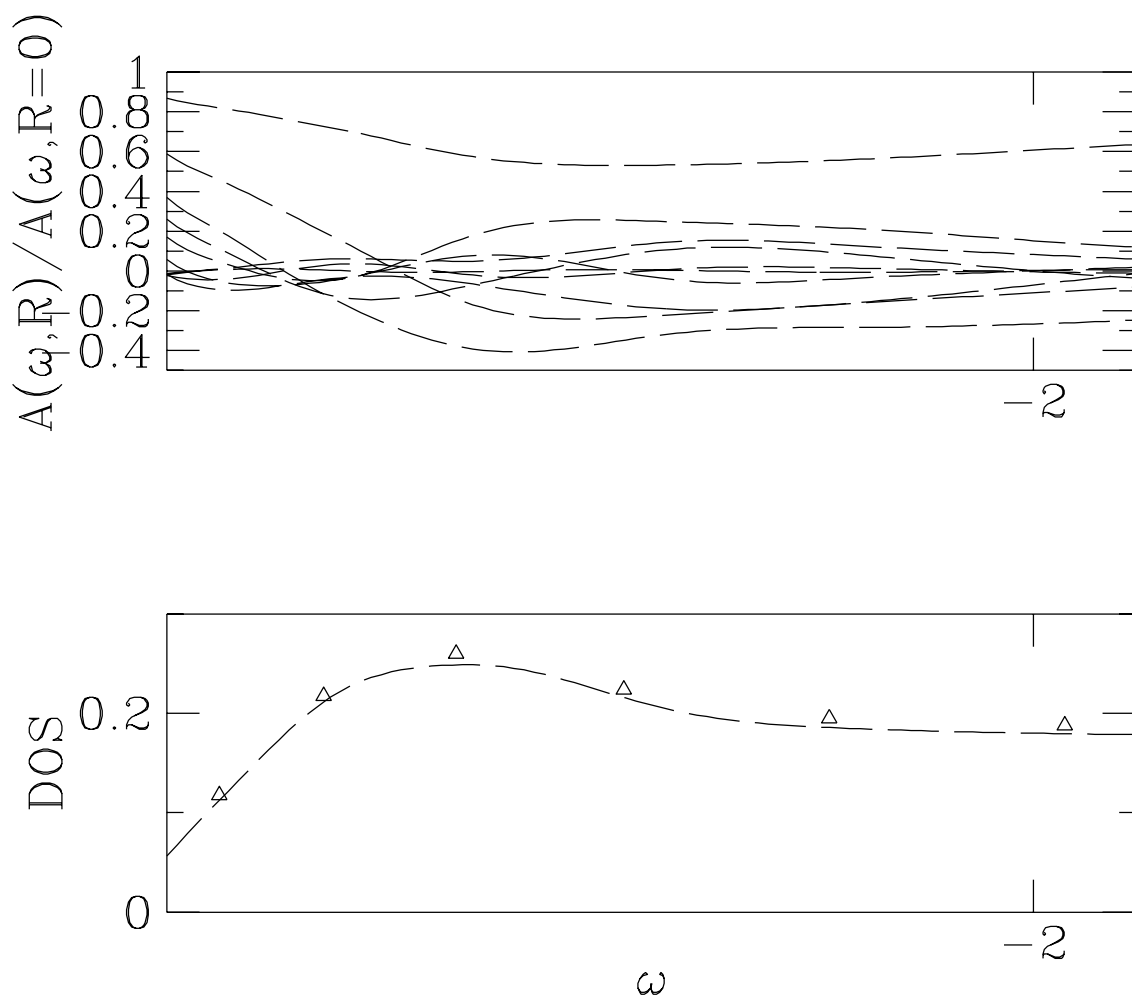
$2n$	$C_n(d^2 = 0)$	$C_n(d^2 = 2)$	$C_n(d^2 = 4)$	$C_n(d^2 = 10)$	$C_n(d^2 = 16)$	$C_n(d^2 = 26)$
32	193448	152314	108676	70960	39081	17614
34	590154	472488	340675	223698	128823	58446
36	1824844	1471492	1068182	708496	414196	196574
38	5677040	4609274	3385018	2264848	1348874	670086
40	17818480	14539266	10760828	7287326	4397638	2245908
42	56220728	46154304	34459409	23573566	14437674	7572526
44	178693158	147425926	110826815	76581474	47561630	25474418
46	570790364	473551402	358473393	249911680	157303528	85932926
48	1834737522	1529492974	1164976270	819090516	521903825	290492088
50	5926011194	4963905566	3804186739	2695446152	1737377480	983973358
52	19240493885	16187397249	12476330859	8905934658	5800668507	3338934862

$2n$	$C_n(d^2 = 36)$	$C_n(d^2 = 50)$	$C_n(d^2 = 64)$	$C_n(d^2 = 82)$	$C_n(d^2 = 100)$	$C_n(d^2 = 122)$	$C_n(d^2 = 144)$	$C(p = 0)$
32	5714	1140	0	0	0	0	0	984446
34	19510	4294	534	0	0	0	0	3087090
36	70917	18258	2981	0	0	0	0	9727036
38	251056	67790	12460	1190	0	0	0	30898232
40	883914	258922	55639	7634	0	0	0	98692630
42	3126095	968326	222326	35058	2661	0	0	317324618
44	10934279	3569044	886787	164380	19237	0	0	1025581138
46	38263835	13147300	3468307	697614	96205	5944	0	3332494632
48	133406362	47855170	13327978	2901958	472897	47830	0	10882673258
50	464563759	173622392	50912034	11813430	2117499	258896	13277	35702392358
52	1616935261	626834742	192138728	47077158	9171222	1332690	117733	117646241223

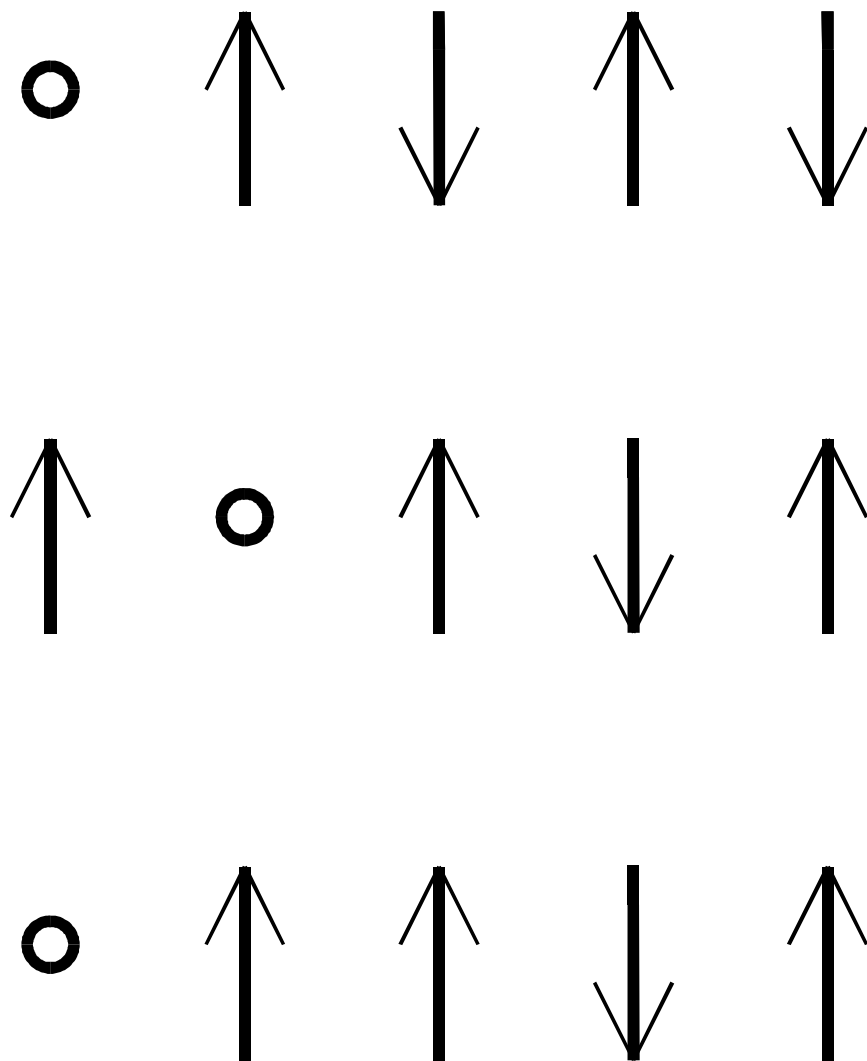
TABLE II. Fit of the coefficients $C_n(R)$ for $R = O$ using the ansatz (46), in the given intervals of n given in the rightmost column.

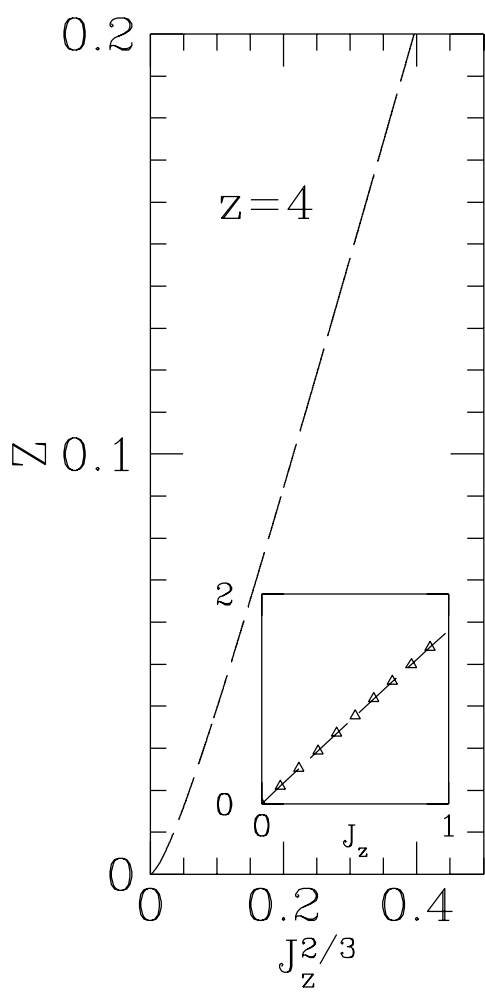
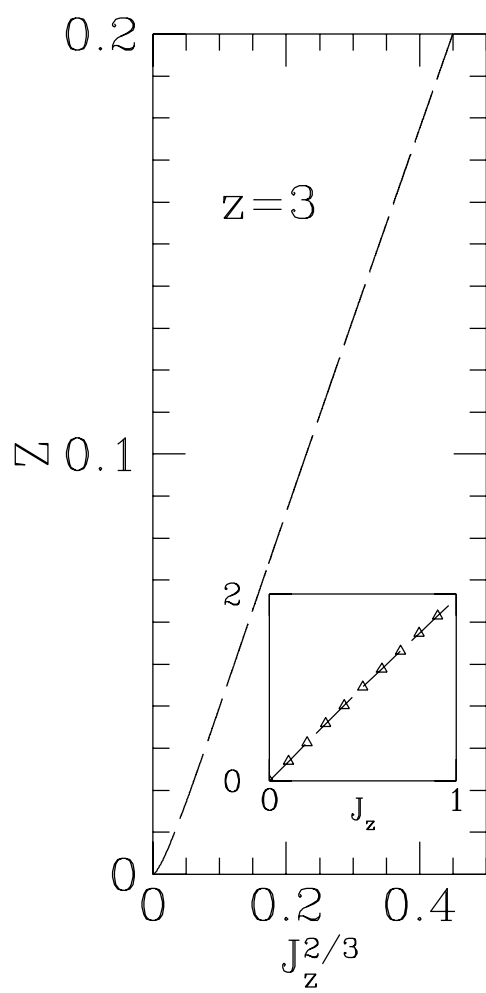
α	$\beta_{R=O}$	$C_{R=O}$	$2n$
1.88136	2.39084	1.26191	22-36
1.88356	2.42844	1.38458	22-38
1.89515	2.63760	2.34793	22-40
1.89049	2.54888	1.86730	22-42
1.89824	2.70449	2.81409	22-44
1.89667	2.67137	2.57441	22-46
1.90428	2.83985	4.08250	22-48
1.90575	2.87370	4.48588	22-50
1.91050	2.98860	6.20875	22-52

α	$\beta_{R=O}$	$C_{R=O}$	$2n$
1.88136	2.39084	1.26191	22-36
1.88399	2.43662	1.41397	24-38
1.89752	2.68445	2.65495	26-40
1.89228	2.58627	2.06374	28-42
1.89925	2.72657	2.98843	30-44
1.89721	2.68362	2.66328	32-46
1.90523	2.86235	4.34957	34-48
1.90657	2.89433	4.75851	36-50
1.91148	3.01404	6.68424	38-52

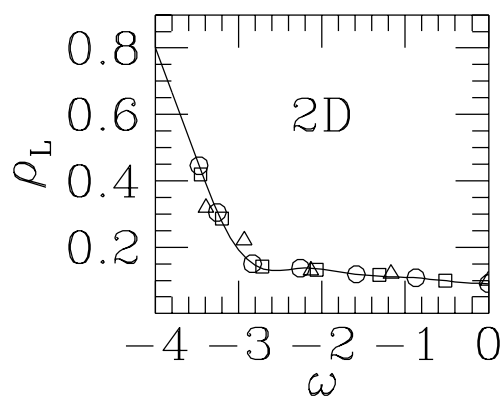
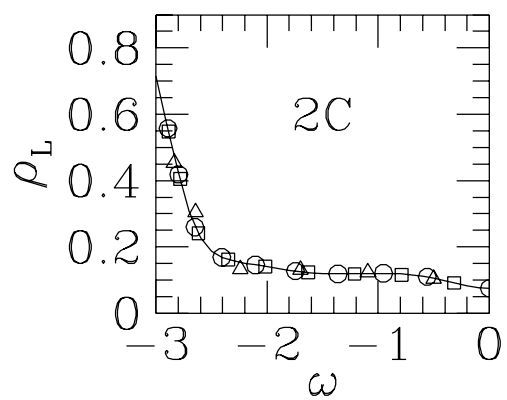
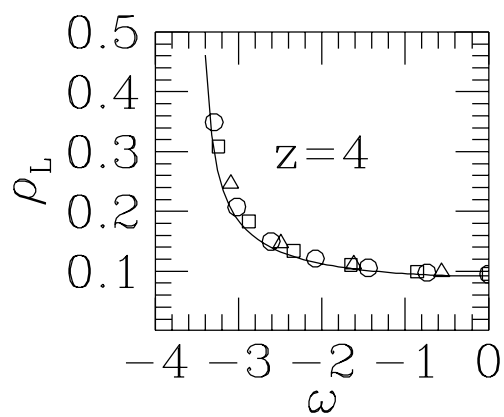
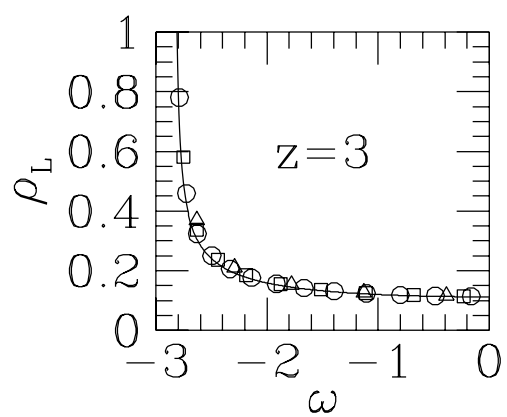


Q.F. Zhong Fig. 1

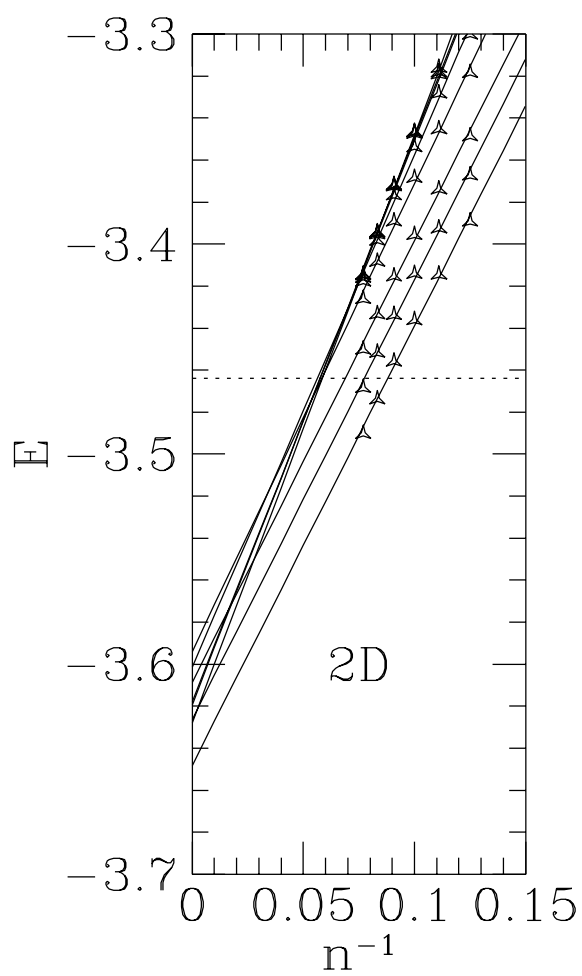
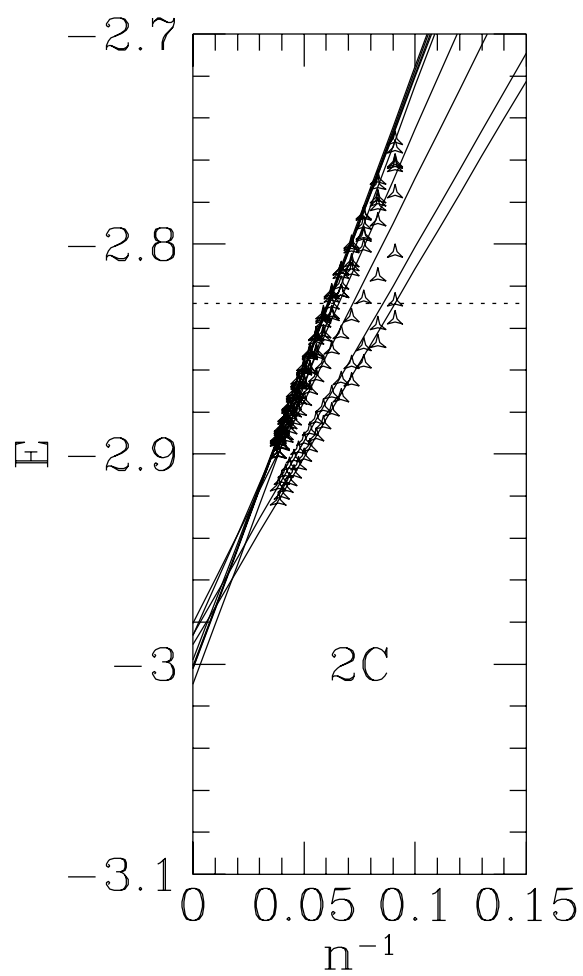




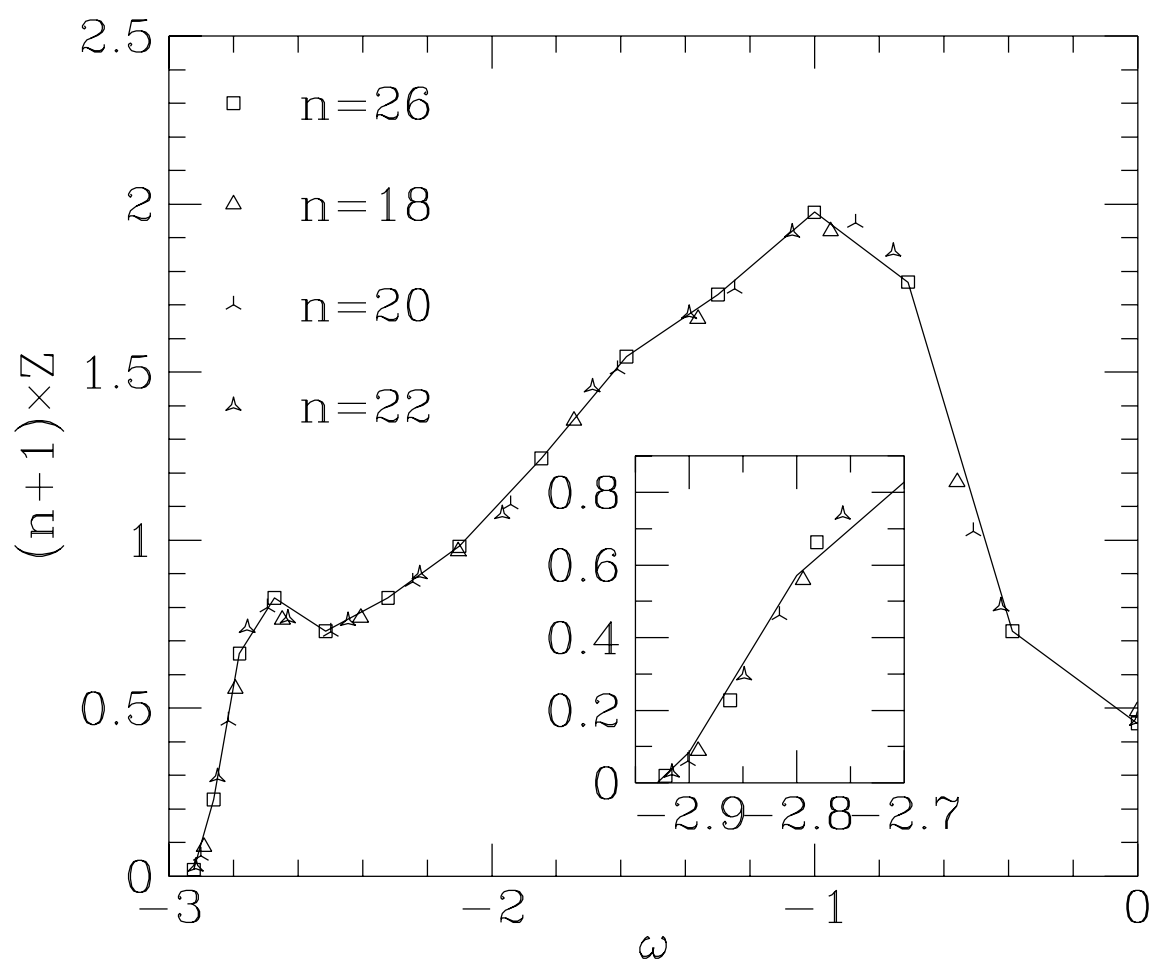
Q.F. Zhong Fig. 3



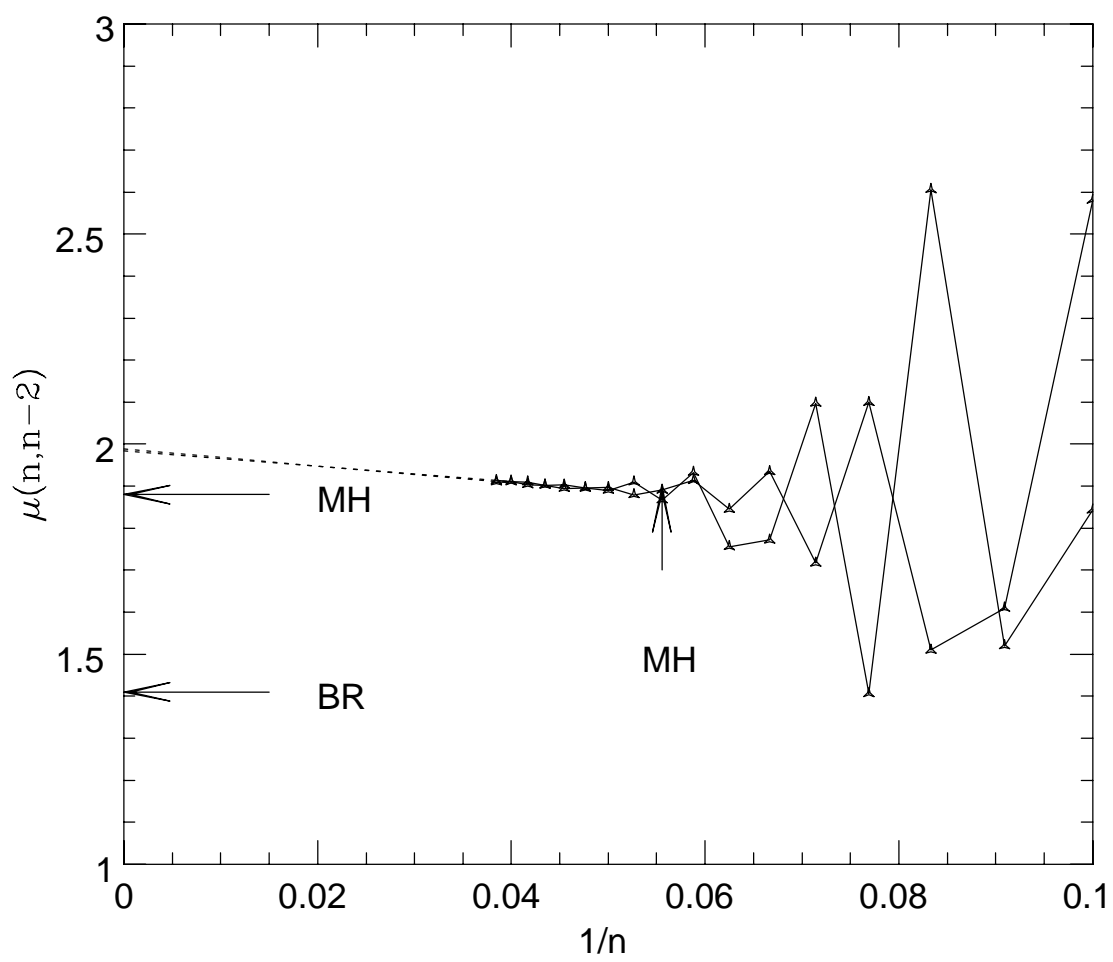
Q.F. Zhong Fig. 4



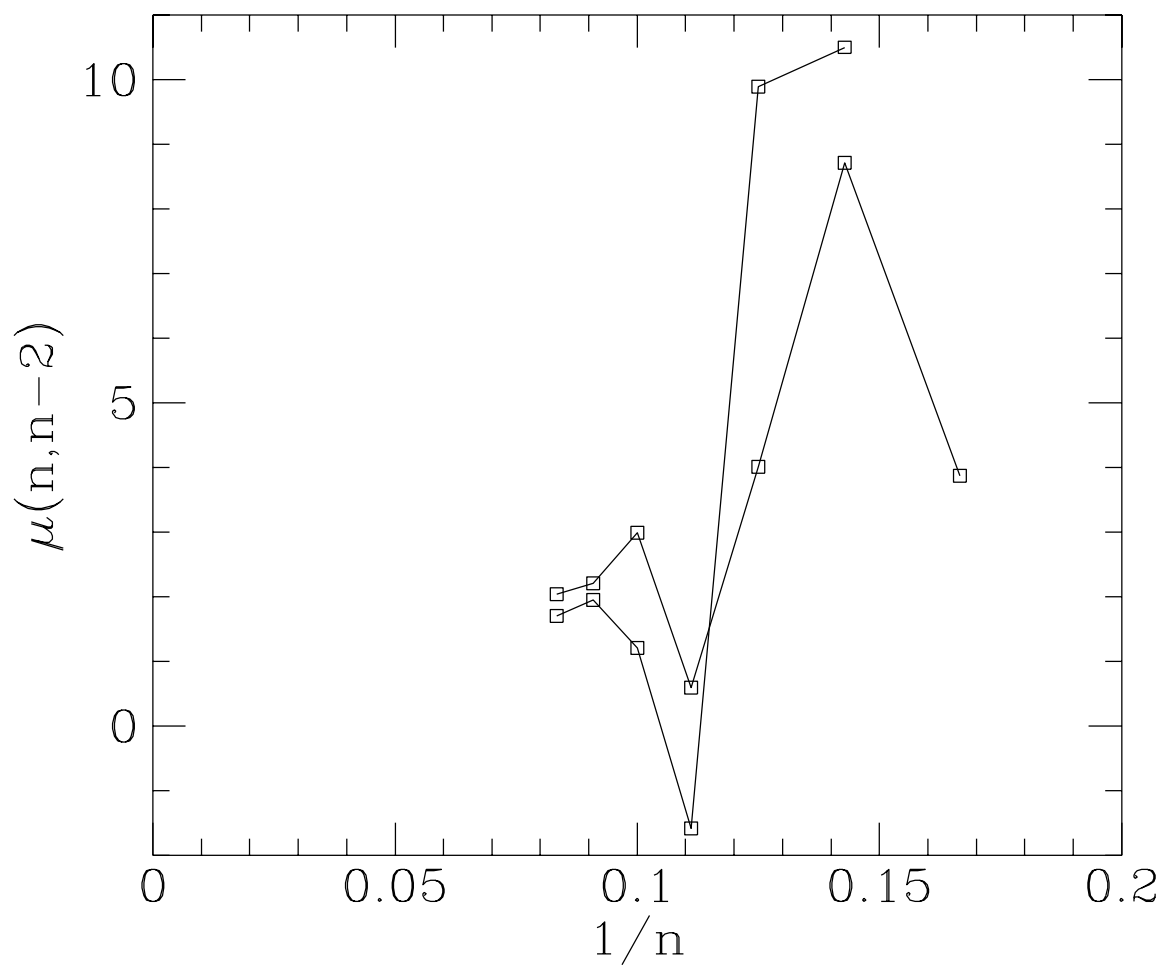
Q.F. Zhong Fig. 5



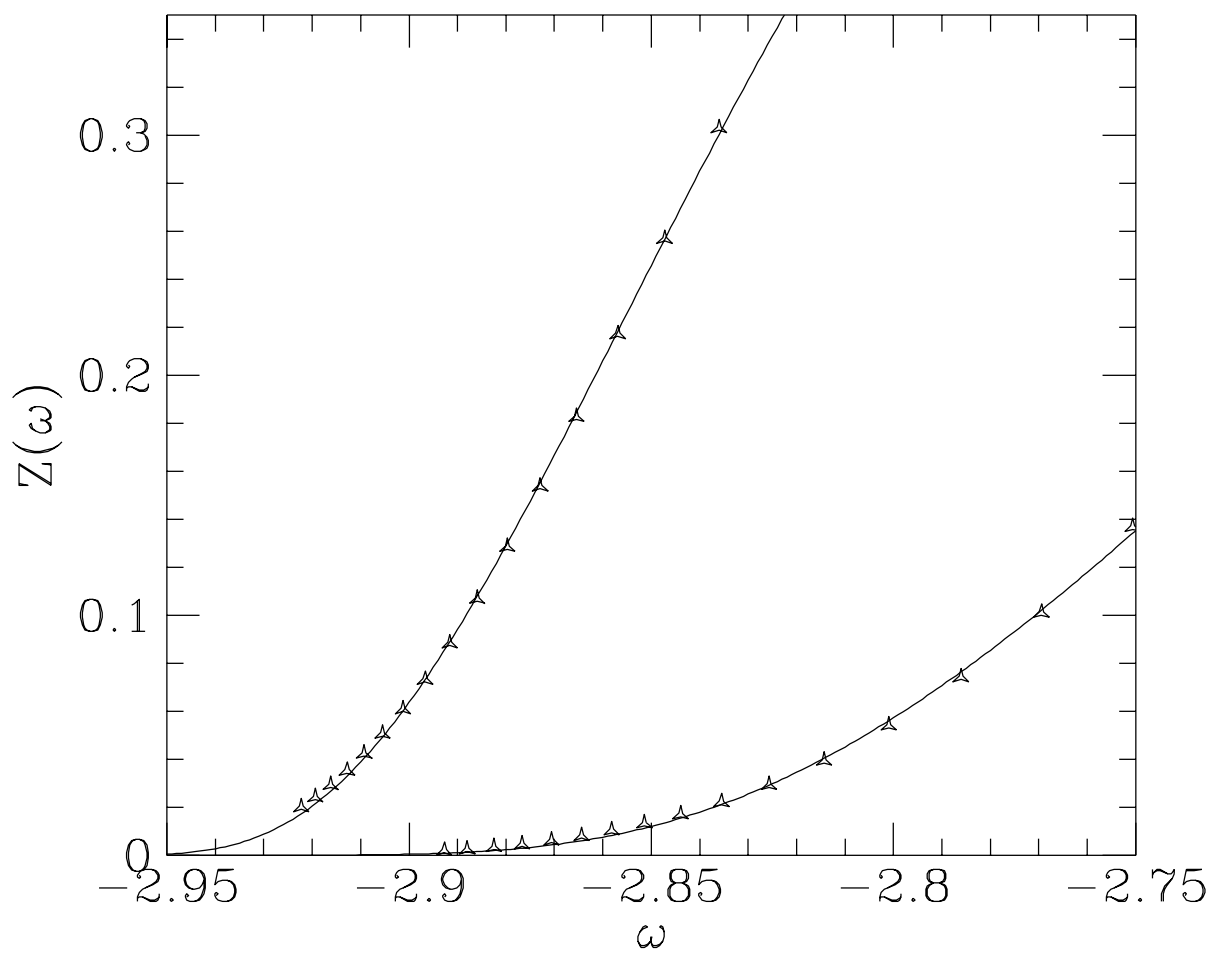
Q.F. Zhong Fig. 6



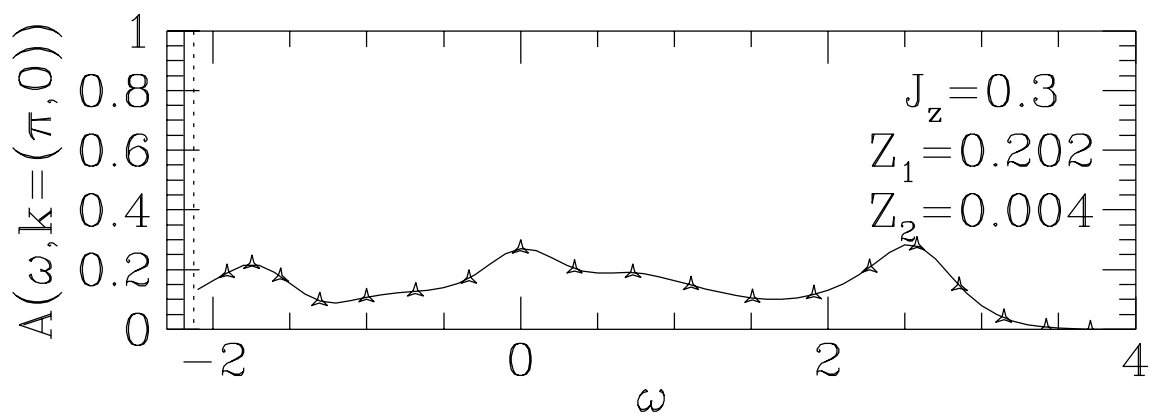
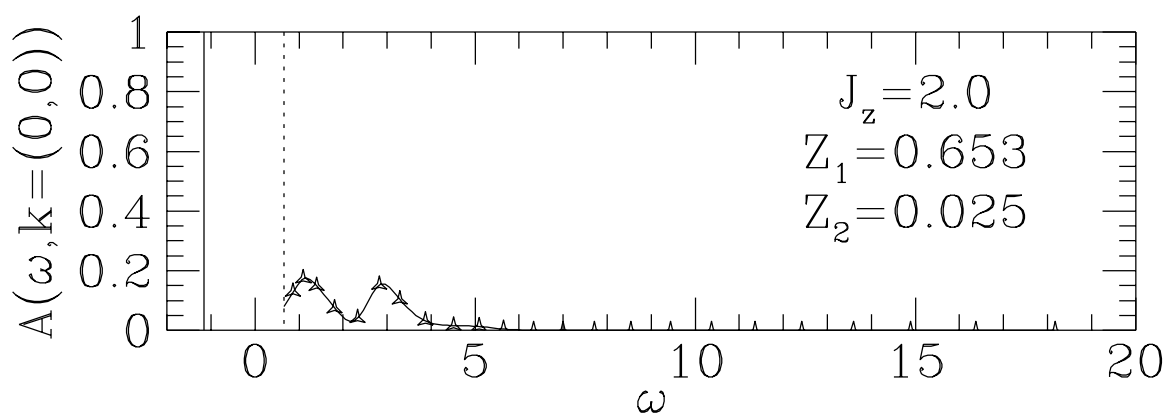
Q.F. Zhong Fig. 7



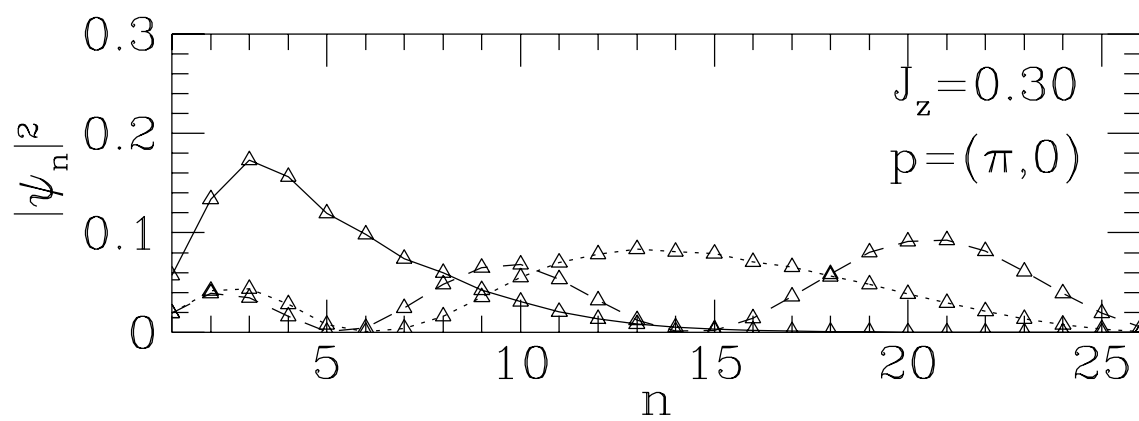
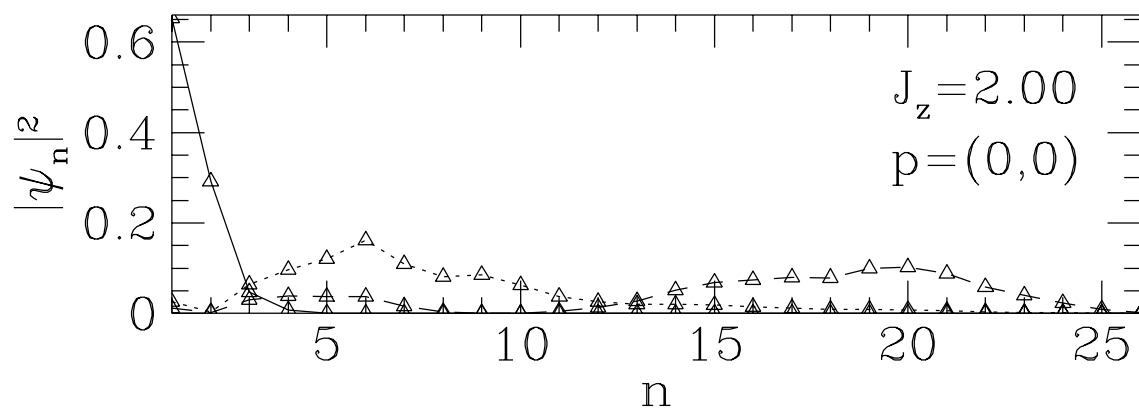
Q.F. Zhong Fig. 8



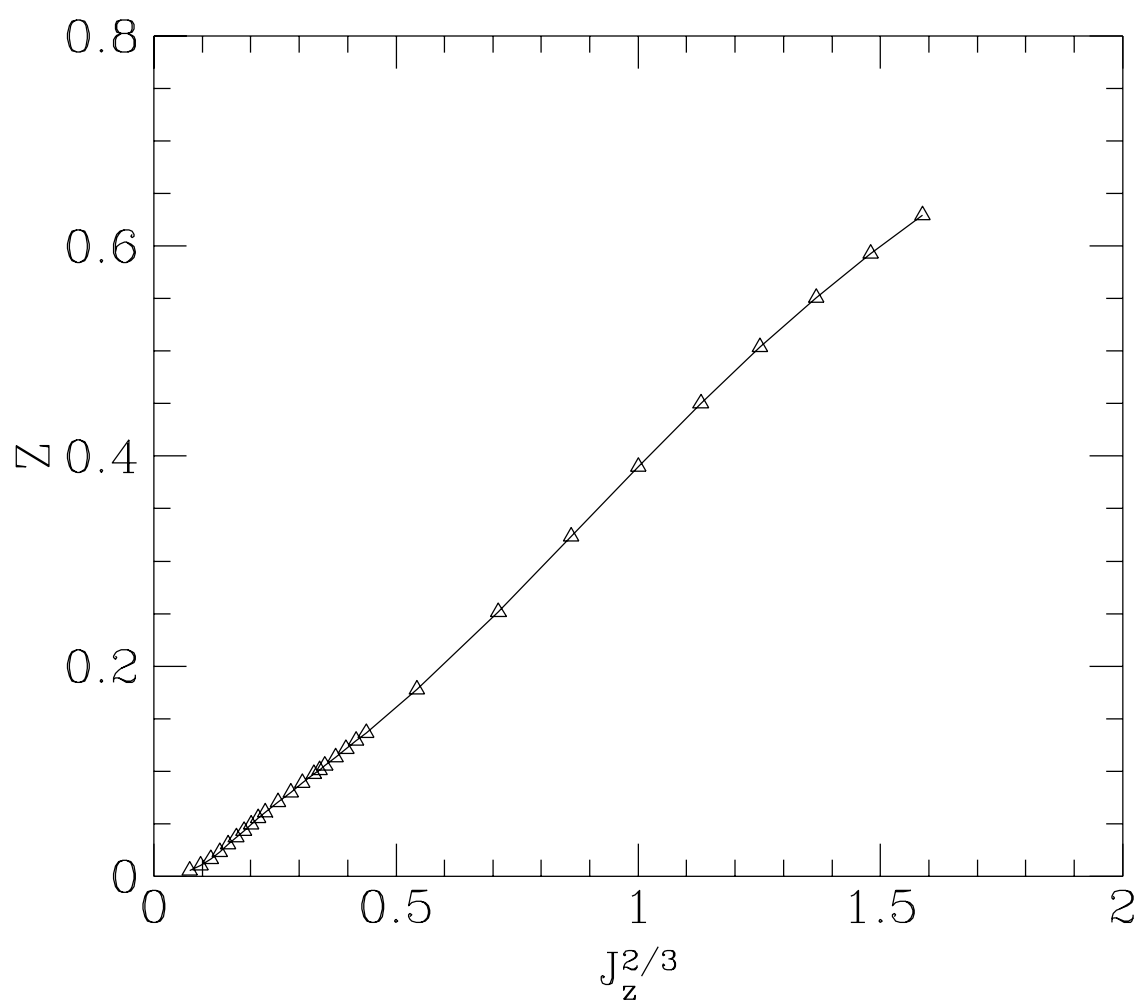
Q.F. Zhong Fig. 9



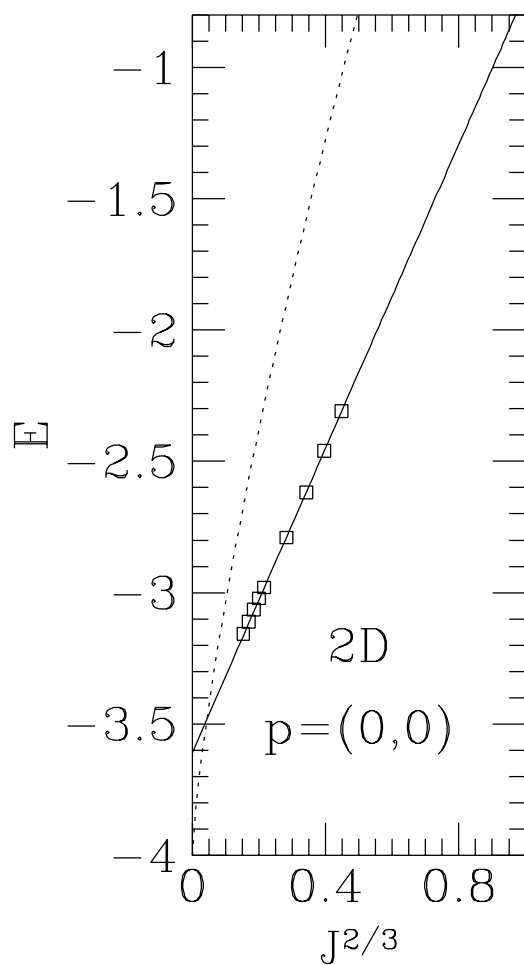
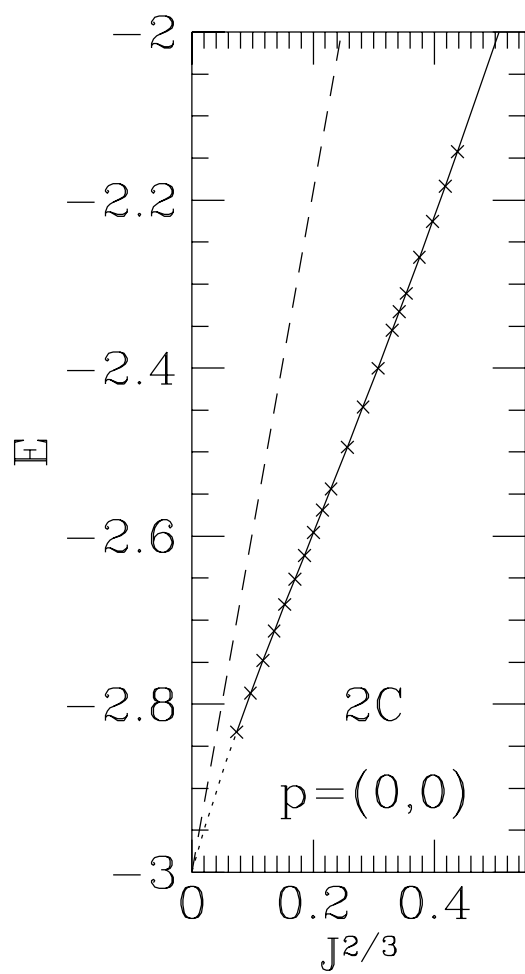
Q.F. Zhong Fig. 10



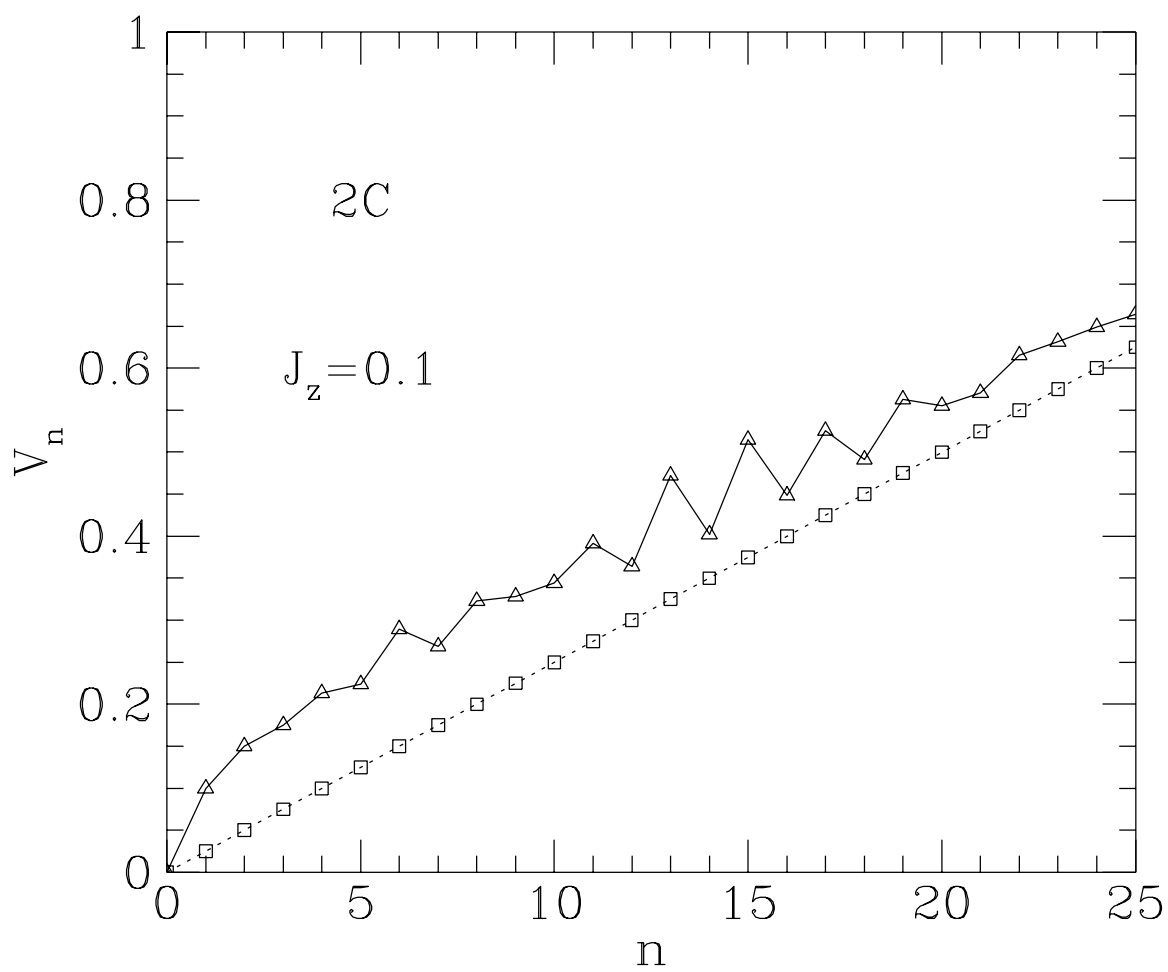
Q.F. Zhong Fig. 11



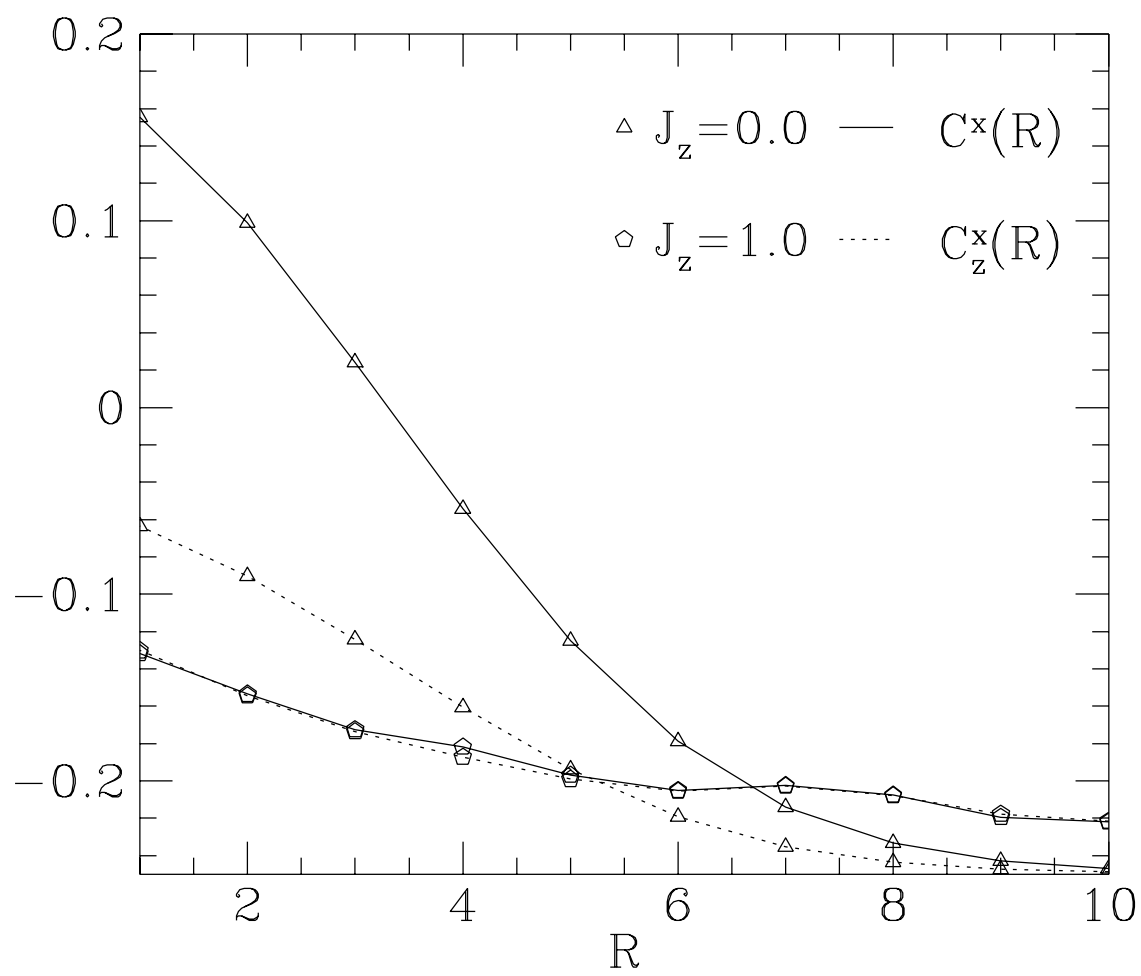
Q.F. Zhong Fig. 12



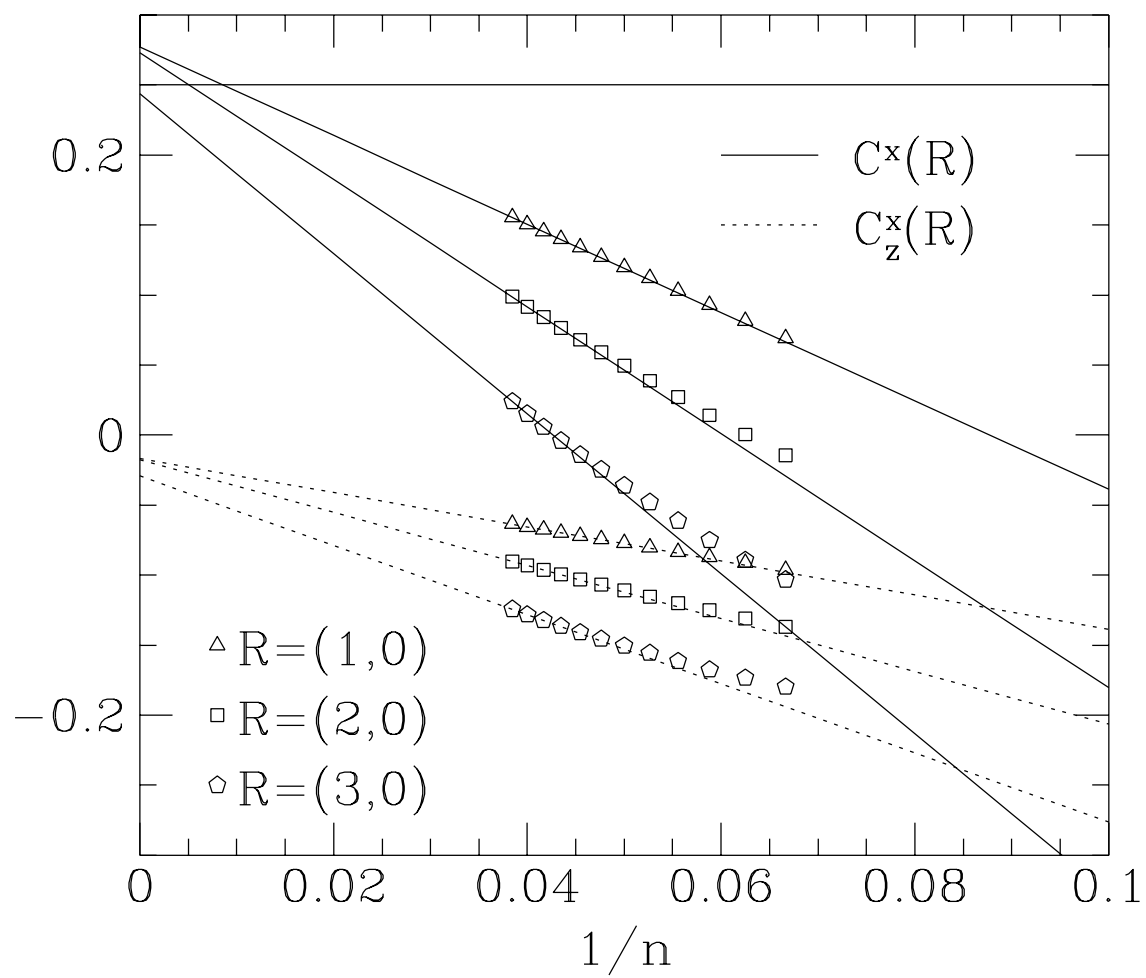
Q.F. Zhong Fig. 13



Q.F. Zhong Fig. 14



Q.F. Zhong Fig. 15



Q.F. Zhong Fig. 16